Advances in Nano Research, *Vol. 18, No. 2 (2025) 143-162*
https://doi.org/10.12989/anr.2025.18.2.143

A shear deformable numerical approaches for the static analysis of bi-directional functionally graded beams

Muhittin Turan[1], Volkan Kahya[2], Ecren Uzun Yaylacı[3] and Murat Yaylacı*[4,5,6]

[1]*Department of Civil Engineering, Bayburt University, 69010 Bayburt, Turkey*
[2]*Department of Civil Engineering, Karadeniz Technical University, 61080, Trabzon, Turkey*
[3]*Faculty of Fisheries, Recep Tayyip Erdogan University, 53100, Rize, Turkey*
[4]*Department of Civil Engineering, Recep Tayyip Erdogan University, 53100, Rize, Turkey*
[5]*Turgut Kıran Maritime Faculty, Recep Tayyip Erdogan University, 53900, Rize, Turkey*
[6]*Murat Yaylacı-Luzeri R&D Engineering Company, 53100, Rize, Turkey*

(*Received November 5, 2024, Revised February 13, 2025, Accepted February 14, 2025*)

Abstract. This paper introduces a highly accurate and computationally efficient shear deformable finite element model for the static analysis of bi-directional functionally graded beams (BD-FGBs) with various boundary conditions grounded in the first-order shear deformation theory (FSDT). The model, featuring ten degrees of freedom across five nodes, excels in capturing both axial and shear deformations with remarkable precision while maintaining a streamlined formulation. In a novel approach, Artificial Neural Network (ANN) methods are also employed alongside the finite element analysis, offering a dual-method investigation into the static behavior of BD-FGBs. This paper aims to further advance the understanding of BD-FGM beams by exploring their static behavior under diverse loading conditions and boundary constraints, employing advanced finite element methods and artificial neural network techniques. The material properties are modeled through power-law distributions, and the governing equations are derived from Lagrange's principle. Displacements and stresses were computed under different boundary conditions (BCs), slenderness ratios (L/h), and power-law indices (p_x, p_z). Comparative analysis with existing literature reveals the superior suitability of the proposed finite element model for static analysis, while the ANN approach further reinforces its potential as a robust, complementary tool. The innovative combination of these methods promises to offer significant contributions to the field and provides new insights into the behavior of BD-FGBs under static loads.
Keywords: bi-directional FGBs; finite element; FSDT; power-law rule; static analysis

1. Introduction

In recent years, functionally graded materials (FGMs) have gained significant attention in structural applications, particularly beam elements, due to their exceptional mechanical properties. Unlike traditional homogeneous materials, FGMs offer a unique advantage with material properties that gradually vary throughout their volume, typically blending metals and ceramics. This gradual variation enhances their resistance to extreme temperatures and mechanical stresses, making them ideal for high-performance applications. Additionally, FGMs offer weight advantages over conventional materials, contributing to more efficient and durable structural designs. Given these superior characteristics, studying the mechanical behavior of FGM-based beams has become a focal point for researchers seeking to leverage their full potential in modern engineering challenges.

The development of the literature reveals a prominent focus on unidirectional functionally graded beams (FGBs), which have been extensively studied. In contrast, bi-directional functionally graded beams (BD-FGBs) have garnered less attention, presenting a valuable area for exploration. Initially, several studies have utilized analytical methods to predict the bending, buckling, and vibration behavior of unidirectional FGBs. For example, using the Euler-Bernoulli beam theory, Sankar (2001) provided an elasticity solution for FGBs subjected to static loads. Li *et al*. (2010) expanded this with an elasticity solution based on higher-order theory for static and dynamic analyses. Aydogdu and Taskin (2007) employed the Navier method to analyze free vibrations in supported FGBs. At the same time, Turan and Kahya (2021) used Navier's method to investigate free vibration and buckling analyses of sandwich FGBs. Numerous analytical solutions have also been published addressing static, buckling, and free vibration behavior under various boundary conditions (Thai *et al*. 2012, Yang *et al*. 2013, Nguyen *et al*. 2015, 2016, Hadi *et al*. 2018, Bennai *et al*. 2022).

In terms of finite element methods (FEM), Filippi *et al*. (2015) utilized finite elements and various theories rooted in the unidirectional Carrera Unified Formulation for static analyses of functionally graded structures. Yarasca *et al*. (2016) developed a Hermite-Lagrangian finite element formulation for the static analysis of single and sandwich FGBs using a highly efficient seven-degree-of-freedom quasi-3D hybrid theory. Kahya and Turan (2017a) proposed a five-node, ten-degree-of-freedom finite element model based on first-order shear deformation theory (FSDT) for

*Corresponding author, Professor,
E-mail: murat.yaylaci@erdogan.edu.tr

ISSN: 2287-237X (Print), 2287-2388 (Online)

free vibration and buckling analyses, followed by further investigations of sandwich FGBs (Kahya and Turan 2018a). Reddy and Nampally (2020) presented a dual mesh finite domain method for bending analysis, and a significant number of recent works have applied FEM for static and dynamic analyses of both functionally graded single and sandwich beams (Kahya and Turan 2017b, 2018b, Lincy Christy *et al*. 2020, Garg *et al*. 2020, Khafaji *et al*. 2020). Finite element analysis has become increasingly urgent in engineering due to its ability to provide cost-effective and rapid computational simulations compared to experimental testing, making it a crucial tool for investigating stress analysis, which has been extensively studied in previous research for its fundamental role in ensuring structural integrity and performance (Ammarullah *et al*. 2022a, b, 2023, Santoso *et al*. 2024).

Given that temperature and stress distributions can manifest in two or three dimensions within beams, unidirectional FGBs may not fulfill these engineering requirements, necessitating the development of bi-directional FGBs. This transition highlights the importance of accurately determining the mechanical behavior of BD-FGBs. Numerous studies in the literature have explored the bending, buckling, and vibration behavior of BD-FGBs through various analytical and numerical approaches based on different beam theories. Noteworthy analytical studies include Lü *et al*. (2008), who employed a state space-based differential quadrature method for bending and thermal deformations of BD-FGBs under various boundary conditions, and Şimşek (2015, 2016), who investigated buckling, accessible, and forced vibration behaviors. Nejad *et al*. (2016a, b) analyzed free vibrations and buckling in BD-FGBs utilizing nonlocal elasticity theory to account for small-scale effects. Other contributions include the work of Shafiei *et al*. (2017), who studied the vibration behavior based on Timoshenko beam theory, and Karamanlı (2017a, b), who investigated bending, buckling, and vibration phenomena in BD-FGBs using various solution methods.

The finite element method is among the most widely employed numerical methods for examining the mechanical behavior of BD-FGBs (Selvamani *et al*. 2024a, b, Civalek *et al*. 2020, Zheng *et al*. 2022, Wang *et al*. 2023, Gul and Aydogdu 2023, Özdemir *et al*. 2024, Huang and Quyang 2020, Turan 2022). For instance, Karamanlı and Vo (2018) utilized FEM and quasi-3D theory to analyze the bending behaviors of micro BD-FGBs, subsequently extending their research to investigate the mechanical behaviors of porous micro BD-FGBs based on variable material length scale parameters (Karamanlı and Vo 2021). Chinh *et al*. (2019) proposed a finite element model for elastostatic bending analysis of sandwich BD-FGBs subjected to various non-uniform loads, while Pham *et al*. (2019) implemented shear deformable finite elements to assess the free and forced vibration behaviors of sandwich BD-FGBs. Chen *et al*. (2020) conducted an isogeometric analysis grounded in Timoshenko beam theory for nonlinear free vibration of rotating porous micro BD-FGBs. Nguyen *et al*. (2020) introduced a BD-FG sandwich beam model made from three distinct materials to study dynamic behaviors under the non-uniform motion of a moving point load. Furthermore, Anh *et al*. (2020) investigated the free vibration of BD-FG sandwich beams using a first-order shear deformation finite element formulation. Viet *et al*. (2020) analyzed the free vibration behavior of cantilever unidirectional and bi-directional FGBs. Le *et al*. (2021) examined buckling and vibration behaviors of sandwich BD-FGBs employing a third-order shear deformation beam element. In recent years, there has been an increase in studies examining the effects of porosity on the mechanical behavior of bi-directional functionally graded (BD-FG) beams. These studies analyze the impact of different porosity distributions on bending, buckling, and vibration behaviors using various beam theories and numerical methods, contributing to the design of lighter and more durable structures (Turan and Adıyaman 2023, 2024, Adiyaman and Turan 2024, Turan 2024). Additionally, there are numerous studies in which different structural types, such as plates, cones, and beams, are modeled using FGM, carbon nanotubes, and composite materials and analyzed through both numerical and analytical methods (Kolahchi *et al*. 2015, 2016, Baseri *et al*. 2016, Hadi Hajmohammad *et al*. 2021, Al-Furjan *et al*. 2022a, b, Furjan *et al*. 2024a, b, 2025, Shan *et al*. 2025).

Recently, there has been a growing interest in integrating Artificial Neural Network (ANN) techniques in analyzing functionally graded beams (FGBs), owing to their ability to model complex relationships and predict behaviors based on large datasets. These advanced computational methods are particularly beneficial in scenarios where traditional analytical and numerical approaches may struggle to capture nonlinearities and intricate interactions within the materials. Studies utilizing ANN methods have demonstrated significant potential in optimizing the design and performance of FGBs under various loading and boundary conditions (Keerthiveettil *et al*. 2024, Sen *et al*. 2024). For instance, researchers have applied ANN algorithms to effectively predict the static and dynamic responses of FGBs, enabling more efficient designs tailored to specific engineering requirements (Truong *et al*. 2020;2021, Turan *et al*. 2023, Bazmara *et al*. 2023, Fallah and Aghdam 2024, Yaylacı *et al*. 2024a, b, c, Sekban *et al*. 2024, Öner *et al*. 2024, Liu *et al*. 2022, Ren *et al*. 2022, Saeed Kamarian *et al*. 2023, Madenci *et al*. 2024, Li *et al*. 2024).

As highlighted in the literature review, research on BD-FGBs using the finite element method (FEM) remains limited, particularly for static analysis. This study stands out by extending the static analysis of bi-directional functionally graded beams (BD-FGBs) using a novel finite element model based on first-order shear deformation theory (FSDT) while uniquely integrating Artificial Neural Network (ANN) methods to enhance computational efficiency and accuracy. While previous studies have primarily focused on buckling and free vibration, this research extends the scope to static analysis, offering an accurate FEM with ten degrees of freedom across five nodes. The effectiveness of this model was rigorously validated through comparisons with established literature, especially for maximum displacements of BD-FGBs. This paper aims to further advance the understanding of BD-

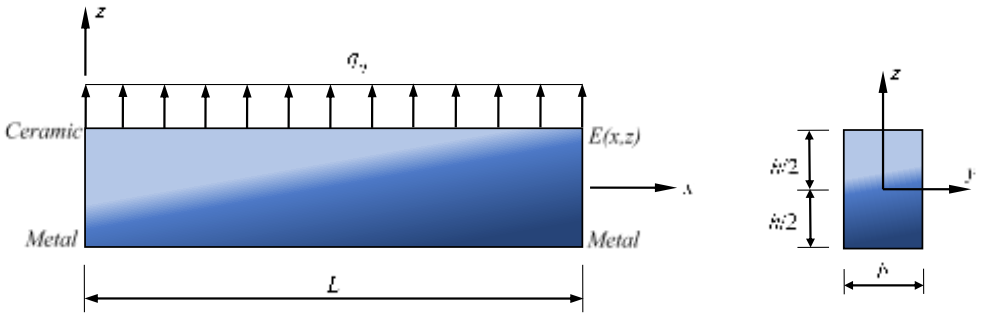

Fig. 1 Coordinates, loading, and geometry of the BD-FGB

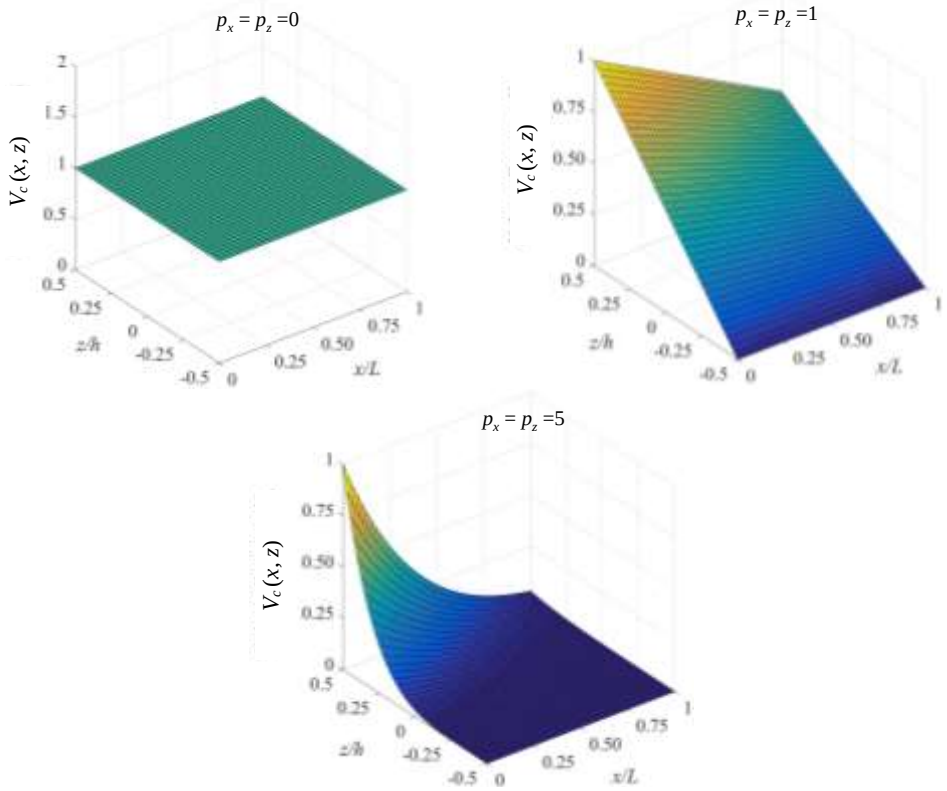

Fig. 2 Changes of $V_c(x,z)$ according to different power-law indexes

FGM beams by exploring their static behavior under diverse loading conditions and boundary constraints, employing advanced finite element methods and artificial neural network techniques. By combining FEM with ANN, this study not only enhances computational efficiency and accuracy but also pushes the boundaries of traditional analysis techniques.

2. Theory and formulation

2.1 Material properties

The coordinates, loading, and geometry of the considered BD-FGBs are shown in Fig. 1. The beam in the figure is made of an isotropic and non-homogeneous linear elastic material (Ammarullah *et al*. 2022, Abd Aziz *et al*. 2024). Here, *L*, *b*, and *h* denote the beam's length, width, and height, respectively. q_0 is the uniformly distributed load on the beam. The material properties of the beam are formed from ceramic (Al_2O_3) and metal (Al). The change of *E* (Young's modulus) and *G* (shear modulus) according to the power law distribution is as follows;

$$\begin{aligned} E(x,z) &= E_m + (E_c - E_m)V_c(x,z) \\ G(x,z) &= G_m + (G_c - G_m)V_c(x,z) \end{aligned} \tag{1}$$

where *m* and *c* (subscripts) represent metal and ceramic, respectively. The effective material properties (*E*, *G*) vary along the *x* and *z* axes of the beam. $V_c(x,z)$, which provides this change according to the power-law rule, is defined as follows.

$$V_c(x,z) = \left(1 - \frac{0.5x}{L}\right)^{p_x} \left(0.5 + \frac{z}{h}\right)^{p_z} \tag{2}$$

where p_x, and p_z are the power-law indexes in the *x* and *z*

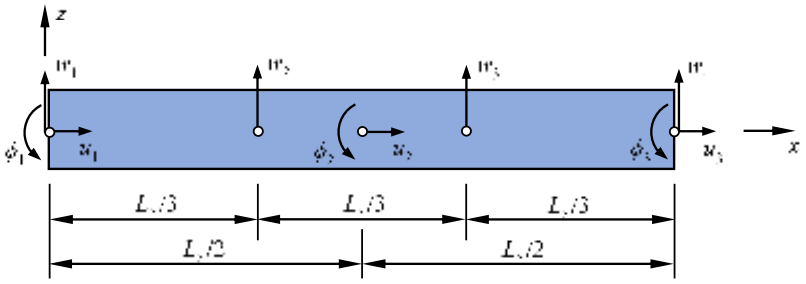

(a)

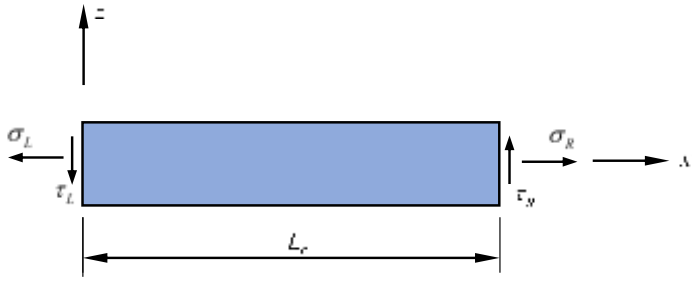

(b)

Fig. 3 a) Beam element with ten DOFs, b) Stress components on the beam element

directions. The changes of $V_c(x,z)$ in the *x* and *z* directions according to different power-law indexes are given in Fig. 2.

2.2 Finite element model and mathematical formulation

A 5-node beam finite element with four equally spaced nodes and a node in the middle is shown in Fig. 3a. This element has 10 degrees of freedom corresponding to 3 axial, 4 transversals, and 3 rotational displacements, which are measured at the neutral axis of the beam. The nodal displacement vector can thus be given by:

$$\boldsymbol{u} = \{u_1 \quad u_2 \quad u_3 \quad w_1 \quad w_2 \quad w_3 \quad w_4 \quad \phi_1 \quad \phi_2 \quad \phi_3\}^T \tag{3}$$

Components of the displacement field of a BD-FGB, according to FSDT, can be written as

$$\begin{aligned} u(x,z) &= u_0(x) + z\,\phi_0(x), \\ w(x,z) &= w_0(x) \end{aligned} \tag{4}$$

The 0 subscript indicates that the variable is on the neutral axis. Normal and shear strains obtained using Eq. (4) are written in Eq. (5). In Eq. (6), the relations of normal and shear stresses are written according to Hooke's law.

$$\begin{aligned} \varepsilon_{xx} &= \frac{\partial u}{\partial x} = \frac{du_0(x)}{dx} + z\frac{d\phi_0(x)}{dx}, \\ \gamma_{xz} &= \frac{\partial u}{\partial z} + \frac{\partial w}{\partial x} = \frac{dw_0(x)}{dx} + \phi_0(x) \end{aligned} \tag{5}$$

$$\sigma_{xx} = E(x,z)\varepsilon_{xx}, \quad \tau_{xz} = KG(x,z)\gamma_{xz} \tag{6}$$

where K is the shear correction factor; ε_{xx}, γ_{xz} is the normal and shear strains; σ_{xx}, τ_{xz} is the normal and shear stresses, respectively.

The strain energy of the beam can be expressed by

$$U = \frac{1}{2}\int_0^{L_e}\int_A (\sigma_{xx}\varepsilon_{xx} + \tau_{xz}\gamma_{xz})dA\,dx \tag{7}$$

where A is the cross-sectional area of the beam. If Eqs. (1), (5), and (6) are substituted into Eq. (7), the strain energy of the beam is written as follows.

$$U = \frac{1}{2}\int_0^{L_e}\begin{bmatrix} A_0\left(\frac{du_0(x)}{dx}\right)^2 + 2A_1\frac{du_0(x)}{dx}\frac{d\phi_0(x)}{dx} \\ +A_2\left(\frac{d\phi_0(x)}{dx}\right)^2 \\ +B_0\left[\left(\frac{dw_0(x)}{dx}\right)^2 + 2\frac{dw_0(x)}{dx}\phi_0 + (\phi_0)^2\right] \end{bmatrix} dx \tag{8}$$

The coefficients in Eq. (8) are as follows.

$$\begin{aligned} [A_0, A_1, A_2] &= \int_A E(x,z)[1, z, z^2]dA\,, \\ B_0 &= \int_A KG(x,z)dA \end{aligned} \tag{9}$$

In Eq. (10), the kinetic energy of the beam is given.

$$T = \frac{1}{2}\int_0^{L_e}\int_A \rho(x,z)(\dot{u}^2 + \dot{w}^2)dA\;dx \tag{10}$$

where the dot shows the concerning derivative according to time. It takes the derivative of Eq. (4) concerning time, replaces it in Eq. (10), and gets Eq. (11).

$$\begin{aligned} T = \frac{1}{2}\int_0^{L_e}\big[&I_0(\dot{u}_0(x))^2 + 2I_1\dot{u}_0(x)\dot{\phi}_0(x) + I_2(\dot{\phi}_0(x))^2 \\ &+ I_0(\dot{w}_0(x))^2\big]dx \end{aligned} \tag{11}$$

where the inertia coefficients are

$$[I_0, I_1, I_2] = \int_A \rho(x,z)[1, z, z^2]dA \tag{12}$$

Moreover, the work done by the non-conservative force $\pi_{n.c.}$ is defined as

$$\pi_{n.c.} = \frac{1}{2}\sum_{i=1}^{m}\left\{\int_{l_i-1}^{l_i}\left[(q_{e,i} - q_{d,i})\bar{w}_i(x,t)\right]dx\right\} \tag{12}$$

The work done by the uniformly distributed load q_0 on the beam is given in Eq. (13).

$$V = \int_0^{L_e} q_0 w_0(x)dx \tag{13}$$

Solutions to $u_0(x)$, $w_0(x)$ and $\phi_0(x)$ can be assumed as

$$\begin{aligned} u_0(x) &= \sum_{i=1}^{3}\varphi_i(x)u_i(t), \\ w_0(x) &= \sum_{i=1}^{4}\psi_i(x)w_i(t), \\ \phi_0(x) &= \sum_{i=1}^{3}\theta_i(x)\phi_i(t) \end{aligned} \tag{14}$$

Here $\varphi_i(x)$, $\psi_i(x)$ and $\theta_i(x)$ are the shape functions, and $u_i(t)$, $w_i(t)$ and $\phi_i(t)$ are the generalized nodal displacements. The quadratic polynomials for $\varphi_i(x)$ and $\theta_i(x)$, and a cubic polynomial for $\psi_i(x)$ obtained by the Lagrange interpolation formula are given explicitly in Appendix A.

The Lagrangian functional is written in Eq. (15).

$$\boldsymbol{H}^{(k)} = \begin{bmatrix} -3E_H & 4E_H & -E_H & 0 & 0 & 0 & 0 & 3E_H z & -4E_H z & E_H z \\ 0 & 0 & 0 & -5.5G_H & 9G_H & -4.5G_H & G_H & -G_H L_e & 0 & 0 \\ E_H & -4E_H & 3E_H & 0 & 0 & 0 & 0 & -E_H z & 4E_H z & -3E_H z \\ 0 & 0 & 0 & -G_H & 4.5G_H & -9G_H & 5.5G_H & 0 & 0 & -G_H L_e \end{bmatrix} \tag{22}$$

$$L = T - (U + V) \tag{15}$$

With the help of Lagrange's equations given in Eq. (16), the governing equations are obtained.

$$\frac{d}{dt}\left(\frac{\partial L}{\partial \dot{q}_i}\right) - \frac{\partial L}{\partial q_i} = 0 \tag{16}$$

where q_i represents the variables of u_i, w_i and ϕ_i. Substituting Eqs. (8), (11) and (13) into Eq. (15) with considering Eq. (14) leads to

$$\begin{bmatrix} m^{11} & 0 & m^{13} \\ 0 & m^{22} & 0 \\ m^{13T} & 0 & m^{33} \end{bmatrix}\begin{Bmatrix} \ddot{u}_i \\ \ddot{w}_i \\ \ddot{\phi}_i \end{Bmatrix} + \begin{bmatrix} k^{11} & 0 & k^{13} \\ 0 & k^{22} & k^{23} \\ k^{13T} & k^{23T} & k^{33} \end{bmatrix}\begin{Bmatrix} u_i \\ w_i \\ \phi_i \end{Bmatrix} = \begin{Bmatrix} 0 \\ f_2 \\ 0 \end{Bmatrix} \tag{17}$$

where **m, k**, and **f** are the element mass matrix, the element stiffness matrix, and the element force vector respectively. **m** and **k** are explicitly given in Appendix A. $\mathbf{f_2}$ is expressed in the following form

$$\boldsymbol{f_2} = \left\{\frac{L_e q_0}{8} \quad \frac{3L_e q_0}{8} \quad \frac{3L_e q_0}{8} \quad \frac{L_e q_0}{8}\right\}^T \tag{18}$$

2.3 Bending analysis

The equation of motion of the BD-FGB is given as follows.

$$\boldsymbol{M\ddot{U}} + \boldsymbol{KU} = \boldsymbol{F} \tag{19}$$

where **U** is the vector of unknowns, **M**, **K**, and **F** are the global mass, stiffness matrix, and global force vector, respectively. For static analysis, **M = 0** in Eq. (19). After imposing the boundary conditions, the system equations given by Eq. (19) have been solved numerically using any numerical method. At the end of this process, displacements are calculated.

2.4 Stresses in one-layer beam element

Finite element stresses are shown in Fig. 3b for the beam element. The normal and shear stresses will be calculated according to Eq. (6), where *K* is ignored. Substituting Eq. (14) into Eq. (5), after some processes, the following matrix equation can be obtained for stresses:

$$\boldsymbol{\sigma}^{(k)} = \boldsymbol{H}^{(k)}\boldsymbol{u}^{(k)} \tag{20}$$

where *k* is the element number (*k*=1,2, … , *N*), **u** contains the local variables of the single element, and **σ** is given by

$$\boldsymbol{\sigma}^{(k)} = \{\sigma_L \quad \tau_L \quad \sigma_R \quad \tau_R\}^T \tag{21}$$

H is a 4×10 matrix given in the following form:

2.5 Artificial neural network training

Artificial neural networks (ANNs) are computer models that resemble human biological neuron structures. ANNs can process data, learn, develop predictions, and make decisions. They can analyze complex relationships more reliably and easily than traditional computer methods (Uzun Yaylacı *et al*. 2022, 2023, Uzun Yaylacı, 2022). In this study, a feed-forward multilayer perceptron (MLP) neural network was used. The training algorithm of the network was Broyden-Fletcher-Goldfarb-Shanno (BFGS). The training set for ANN was obtained from experimental data of a total of 145 designs. Three different parameters were used as input to the network. These are as follows:

p_x, p_z: Power-law indexes

L/h: Slenderness

The output layer of the network consists of three parameters. These are normal stresses, shear stresses, and maximum displacements.

Data processing and design of artificial neural networks

Table 1 Training characteristics of ANN

Network	MLP	Error in learning (%)	Error in Testing (%)	Error in validation (%)	Learning algorithm	Error function	Activation function in hidden layer	Activation function in output layer
N_1	3-13-3	1.33	0	0	BFGS 368	sos	Exponential	Identity
N_2	3-13-3	0.97	0.87	3.54	BFGS 234	sos	Exponential	Identity
N_3	3-15-3	1.56	0	1.41	BFGS 267	sos	Exponential	Identity

Table 1 Training characteristics of ANN

BCs	Number of elements, *N*										Ref. 2
	4	6	8	10	12	14	16	18	20	22	
SS	9.4838	9.8005	9.9209	9.9765	10.0044	10.0101	10.0176	10.0214	10.0236	10.0251	10.0074
CC	2.5243	2.6176	2.6599	2.6771	2.6852	2.6868	2.6890	2.6901	2.6907	2.6912	2.6014
CF	76.9558	78.8637	79.6169	80.0168	80.2228	80.2644	80.3202	80.3482	80.3651	80.3763	80.3606

*Ref. 2: Turan (2022)

were performed using the "Artificial Neural Network" module in Statistica software 12. The module categorized the data entered into the system as 70% for the learning group, 15% for the testing group, and 15% for the validation group. The number of hidden layers and neurons was calculated by trial and error, and the weights were assigned random values between 0.0001 and 0.001. Then, the network activation functions (Identity, logistic sigmoid, hyperbolic tangent, exponential, softmax, and Gaussian) were selected, and 12000 networks were trained/retrained. The program code was rewritten in C++ to calculate the normal stresses, shear stresses, and maximum displacements.

3. Results and discussion

This section gives comprehensive results to examine the effects of power-law indexes (p_x, p_z), slenderness (L/h), and BCs on static analysis of BD-FGBs. The present finite element is verified with some numerical examples and validated through ANN. In addition, comprehensive results that can be reference data for future studies are presented under the title of parametric study. In solving the problem, the length is L=1m, and the width is b=0.1m. Two different slenderness such that L/h = 5 and 20 are considered. q_0 is 10,000 N/m. BD-FGB is formed from aluminum (Al) as metal and alumina (Al_2O_3) as ceramic. Their material properties are respectively E_m = 70GPa, ρ_m = 2702kg/m^3, ν_m = 0.3, E_c = 380GPa, ρ_c = 3960kg/m^3, and ν_c = 0.3. BCs for the beam are assumed to be clamped-clamped (CC), simply supported (SS), and clamped-free (CF). The shear correction factor is considered to be K = 5/6 for a rectangular cross-section. This study gives the displacements, normal, and shear stresses in the following non-dimensional form.

$$\bar{w} = \frac{100E_m bh^3}{q_0 L^4} w(x,0), \quad \bar{\sigma}_{xx} = \frac{bh}{q_0 L}\sigma_{xx}(x,z), \quad \bar{\tau}_{xz} = \frac{bh}{q_0 L}\tau_{xz}(x,z) \tag{23}$$

Here, m and c (subscripts) represent metal and ceramic, respectively. Additionally, in this study, a neural network model was developed to estimate normal stresses, shear stresses, and maximum displacements. The error term was accepted as sos. The exponential activation function in the hidden layer and the Identity activation function in the output layer produced the most accurate prediction. The superior networks were obtained with 13 and 15 hidden layers. The result showed that the developed network model provided fast and simple predictions. The characteristics of the best network are shown in Table 1.

3.1 Convergence and verification study

A convergence study was conducted to determine the optimal number of finite elements required to solve the problem accurately. Table 2 presents the variation in non-dimensional maximum displacements of BD-FGBs as a function of finite element numbers under different boundary conditions (BCs). In this analysis, the parameters were set to L/h = 5 and p_x=p_z=2. As evident from the table, the results converge as the number of finite elements increases. Based on this study, it was determined that using 14 elements provides results with the desired level of accuracy. Additionally, the outcomes of this study were compared with those of Turan (2022), who employed a Navier-type solution, and a strong agreement between the two sets of results was observed.

Tables 3 and 4 present the validation of non-dimensional maximum displacements for bi-directional functionally graded beams (BD-FGBs) under various boundary conditions (BCs) and power-law indexes, with slenderness ratios of L/h = 5 and L/h = 20, respectively. The results of this study are compared with those from Huang and Ouyang (2020), Turan (2022), and the Artificial Neural Network (ANN) model used in this research. Huang and Ouyang used an exact solution based on Timoshenko beam theory, while Turan employed a Navier-type analytical solution grounded in first-order shear deformation theory (FSDT). The comparison demonstrates strong agreement between

Table 3 Verification of non-dimensional maximum displacements of the BD-FGBs (L/h = 5)

BCs			p_x =0	p_x =0.5	p_x =1	p_x =2	p_x =5
SS	p_z =0	Present (FEM)	3.1657	3.5667	4.0133	5.0352	8.5894
		Present (ANN)	3.15493662	3.55885326	4.00728005	5.02613664	8.58252848
		Ref. 2	3.1657	3.5696	4.0155	5.0247	8.5094
		Ref. 1	3.165658	3.570196	4.018162	5.035384	8.54317
	p_z =0.5	Present (FEM)	4.8349	5.3504	5.9006	7.0757	10.5284
		Present (ANN)	4.80927503	5.33327872	5.88997892	7.05588804	10.51681876
		Ref. 2	4.8349	5.3544	5.9045	7.0688	10.4737
		Ref. 1	4.834847	5.355052	5.907710	7.081084	10.51150
	p_z =1	Present (FEM)	6.2599	6.8041	7.3658	8.5115	11.6101
		Present (ANN)	6.24612822	6.78504852	7.33780996	8.5046908	11.59384586
		Ref. 2	6.2600	6.8082	7.3702	8.5064	11.5713
		Ref. 1	6.259923	6.809204	7.374088	8.520527	11.60851
	p_z =2	Present (FEM)	8.0303	8.5236	9.0213	10.0101	12.6020
		Present (ANN)	7.99657274	8.50058628	8.98882332	10.00409394	12.5856174
		Ref. 2	8.0304	8.5274	9.0252	10.0074	12.5844
		Ref. 1	8.030299	8.528547	9.029599	10.021390	12.61090
	p_z =5	Present (FEM)	9.6483	10.0760	10.5094	11.3705	13.5826
		Present (ANN)	9.63672204	10.0467796	10.48207556	11.35344425	13.54049394
		Ref. 2	9.6485	10.0798	10.5147	11.3769	13.5941
		Ref. 1	9.648317	10.080426	10.517250	11.382810	13.59786
CC	p_z =0	Present (FEM)	0.8630	0.9780	1.1025	1.3716	2.1277
		Present (ANN)	0.8591165	0.9752616	1.09665675	1.36926828	2.12323183
		Ref. 2	0.8547	0.9647	1.0737	1.2816	1.9214
		Ref. 1	0.863026	0.978111	1.100220	1.356669	2.049671
	p_z =0.5	Present (FEM)	1.2827	1.4288	1.5803	1.8859	2.6255
		Present (ANN)	1.27949325	1.4237992	1.57808758	1.87552755	2.61526055
		Ref. 2	1.2713	1.4119	1.5471	1.7945	2.5143
		Ref. 1	1.282729	1.429198	1.578524	1.873337	2.571593
	p_z =1	Present (FEM)	1.6403	1.7968	1.9541	2.2586	2.9434
		Present (ANN)	1.63357477	1.79212832	1.95038721	2.25656726	2.9227962
		Ref. 2	1.6262	1.7773	1.9191	2.1707	2.8374
		Ref. 1	1.640251	1.797394	1.953105	2.249226	2.905973
	p_z =2	Present (FEM)	2.1101	2.2605	2.4085	2.6868	3.2810
		Present (ANN)	2.09933849	2.2564311	2.40151535	2.68384452	3.2770628
		Ref. 2	2.0918	2.2369	2.3703	2.6014	3.1623
		Ref. 1	2.110060	2.261353	2.408455	2.681505	3.259906
	p_z =5	Present (FEM)	2.6477	2.7839	2.9158	3.1560	3.6347
		Present (ANN)	2.64319891	2.78000254	2.90442838	3.152844	3.63251918
		Ref. 2	2.6216	2.7529	2.8723	3.0761	3.5429
		Ref. 1	2.647691	2.784842	2.916499	3.154211	3.627800
CF	p_z =0	Present (FEM)	28.7811	30.1179	31.5378	34.6207	45.3295
		Present (ANN)	28.73217213	30.07573494	31.50941598	34.56876895	45.27963755
		Ref. 2	28.7473	30.1186	31.5755	34.7396	45.7295
		Ref. 1	28.78105	30.15195	31.60848	34.77199	45.76062
	p_z =0.5	Present (FEM)	44.2042	45.9405	47.7418	51.5063	63.3067
		Present (ANN)	44.01854236	45.77970825	47.69883238	51.43419118	63.23832876

Table 3 Continued

BCs			p_x =0	p_x =0.5	p_x =1	p_x =2	p_x =5
CF	p_z =1	Ref. 2	44.1577	45.9387	47.7866	51.6488	63.7482
		Ref. 1	44.20422	45.98466	47.83211	51.69343	63.79118
		Present (FEM)	57.3774	59.2207	61.0973	64.9131	76.1985
		Present (ANN)	57.2339565	58.90683029	60.98121513	64.64695629	76.11468165
		Ref. 2	57.3202	59.2108	61.1355	65.0491	76.6154
		Ref. 1	57.37739	59.26747	61.19166	65.10426	76.66856
	p_z =2	Present (FEM)	73.5629	75.2324	76.9094	80.2644	89.9307
		Present (ANN)	73.45255565	75.09698168	76.57868958	80.16808272	89.8407693
		Ref. 2	73.4886	75.2007	76.9204	80.3606	90.2656
		Ref. 1	73.56287	75.27434	76.99351	80.43270	90.33556
	p_z =5	Present (FEM)	87.5977	89.0348	90.4865	93.4053	101.8049
		Present (ANN)	87.44878391	88.82111648	90.24218645	93.05970039	101.4384024
		Ref. 2	87.4922	88.9659	90.4545	93.4475	102.0546
		Ref. 1	87.59765	89.07082	90.55890	93.55095	102.15620

*Ref. 1: Huang and Ouyang (2020), *Ref. 2: Turan (2022)

Table 4 Verification of non-dimensional maximum displacements of the BD-FGBs (L/h = 20)

BCs			p_x =0	p_x =0.5	p_x =1	p_x =2	p_x =5
SS	p_z =0	2.8963	3.2598	3.6626	4.5805	7.8135	2.8963
		2.88877	3.253606	3.659304	4.548437	7.773651	2.88877
		2.8963	3.2641	3.6717	4.6004	7.8653	2.8963
		2.896250	3.263220	3.668114	4.585229	7.79113	2.896250
	p_z =0.5	4.4648	4.9341	5.4327	6.4941	9.6524	4.4648
		4.46122816	4.91732406	5.42074806	6.48435885	9.63502568	4.46122816
		4.4648	4.9395	5.4438	6.5166	9.7009	4.4648
		4.464817	4.938653	5.440275	6.503195	9.65205	4.464817
	p_z =1	5.8049	6.2975	6.8038	7.8336	10.6640	5.8049
		5.796773	6.27294	6.796996	7.8289	10.61921	5.796773
		5.8049	6.3031	6.8149	7.8553	10.7071	5.8049
		5.804923	6.302432	6.812172	7.845432	10.67415	5.804923
	p_z =2	7.4397	7.8766	8.3166	9.1940	11.5594	7.4397
		7.42110075	7.83485402	8.30079846	9.1563046	11.54668466	7.42110075
		7.4397	7.8816	8.3262	9.2125	11.5963	7.4397
		7.439674	7.881153	8.324664	9.206755	11.57536	7.439674
	p_z =5	8.8069	9.1798	9.5616	10.3342	12.3931	8.8069
		8.772553	9.17062	9.555863	10.2908	12.34972	8.772553
		8.8069	9.1840	9.5700	10.3510	12.4264	8.8069
		8.806879	9.183795	9.569164	10.346860	12.41100	8.806879
CC	p_z =0	Present (FEM)	0.5936	0.6721	0.7563	0.9359	1.4370
		Present (ANN)	0.592116	0.66974765	0.75524118	0.93075255	1.4313957
		Ref. 2	0.5931	0.6694	0.7450	0.8896	1.3350
		Ref. 1	0.593618	0.672502	0.755911	0.930423	1.403893
	p_z =0.5	Present (FEM)	0.9127	1.0137	1.1169	1.3215	1.8117
		Present (ANN)	0.911148	1.012281	1.115895	1.319518	1.809707
		Ref. 2	0.9119	1.0106	1.1052	1.2779	1.7787
		Ref. 1	0.912698	1.014243	1.116901	1.317594	1.791193

Table 4 Continued

BCs			p_x =0	p_x =0.5	p_x =1	p_x =2	p_x =5
CC	p_z =1	Present (FEM)	1.1853	1.2913	1.3960	1.5952	2.0440
		Present (ANN)	1.183878	1.286393	1.391952	1.591052	2.040934
		Ref. 2	1.1843	1.2883	1.3853	1.5563	2.0099
		Ref. 1	1.185251	1.291978	1.396487	1.593176	2.031677
	p_z =2	Present (FEM)	1.5194	1.6143	1.7068	1.8813	2.2694
		Present (ANN)	1.516665	1.612524	1.70441	1.873399	2.263273
		Ref. 2	1.5182	1.6112	1.6963	1.8438	2.2105
		Ref. 1	1.519435	1.615071	1.707730	1.881155	2.264002
	p_z =5	Present (FEM)	1.8063	1.8883	1.9702	2.1263	2.4614
		Present (ANN)	1.803049	1.887167	1.964683	2.115031	2.459431
		Ref. 2	1.8045	1.8842	1.9581	2.0880	2.4024
		Ref. 1	1.806252	1.888996	1.971252	2.126988	2.460596
CF	p_z =0	Present (FEM)	27.7034	28.9526	30.2767	33.1448	43.1155
		Present (ANN)	27.58982	28.92075	30.23128	33.08514	43.08101
		Ref. 2	27.7008	28.9828	30.3420	33.2873	43.5259
		Ref. 1	27.70342	28.98523	30.34430	33.28938	43.52787
	p_z =0.5	Present (FEM)	42.7241	44.3514	46.0364	49.5510	60.5836
		Present (ANN)	42.42503	44.12521	45.95353	49.4073	60.51696
		Ref. 2	42.7204	44.3903	46.1197	49.7272	61.0459
		Ref. 1	42.72410	44.39376	46.12296	49.73018	61.04855
	p_z =1	Present (FEM)	55.5574	57.2783	59.0267	62.5759	73.1023
		Present (ANN)	55.47406	57.02055	58.86143	62.24425	72.97803
		Ref. 2	55.5528	57.3187	59.1129	62.7549	73.5496
		Ref. 1	55.55739	57.32303	59.11699	62.75864	73.55288
	p_z =2	Present (FEM)	71.2004	72.7343	74.2737	77.3553	86.3153
		Present (ANN)	71.0224	72.47973	74.16972	76.92985	85.97867
		Ref. 2	71.1944	72.7684	74.3479	77.5097	86.6972
		Ref. 1	71.20037	72.77410	74.35345	77.51483	86.70173
	p_z =5	Present (FEM)	84.2319	85.5351	86.8576	89.5375	97.3971
		Present (ANN)	84.01289706	85.37258331	86.77942816	88.9107375	96.90037479
		Ref. 2	84.2237	85.5610	86.9181	89.6680	97.7267
		Ref. 1	84.23190	85.56895	86.92588	89.67549	97.73379

*Ref. 1: Huang and Ouyang (2020), *Ref. 2: Turan (2022)

this study's findings, the referenced works, and the ANN predictions, highlighting the accuracy and reliability of the proposed finite element method. For both slenderness ratios (L/h = 5 and L/h = 20), the smallest displacements are observed when the power-law indexes $p_x = p_z = 0$, corresponding to a fully ceramic beam. As the power-law indexes increase, the displacements grow in both directions, indicating that a higher metal content leads to greater flexibility. Additionally, as the slenderness ratio increases, the non-dimensional maximum displacements decrease. Among the boundary conditions, the smallest displacements are observed for clamped-clamped (CC) beams, while the largest displacements occur when clamped-free (CF) boundary conditions are applied, reflecting the higher flexibility of CF configurations. The results from the ANN model further confirm these trends, providing additional validation for the accuracy of the analysis.

Table 5 provides the verification of non-dimensional normal and shear stresses for simply supported bi-directional functionally graded beams (BD-FGBs) under various power-law indexes. The results of this study are compared with both the Artificial Neural Network (ANN) model and the findings from Ref. 2, showing strong agreement across all cases. The analysis reveals that normal stresses increase as the power-law index p_z increases, except when $p_z = 0$, where the beam is fully ceramic. Conversely, normal stresses decrease with increasing values of p_x. As the slenderness ratio increases, normal stresses also rise,

Table 5 Verification of non-dimensional normal and shear stresses of the SS BD-FGBs

			p_x =0	p_x =1	p_x =2	p_x =5
			$\bar{\sigma}_{xx}(\frac{L}{2},\frac{h}{2})$			
L/*h*=5	p_z =0	Present (FEM)	3.7503	3.7502	3.7503	3.7503
		Present (ANN)	3.74579964	3.74195	3.744675	3.74505
		Ref. 2	3.7507	3.7509	3.7511	3.7508
	p_z =1	Present (FEM)	5.7962	5.5436	5.2955	4.6469
		Present (ANN)	5.77939102	5.535285	5.290734	4.627383
		Ref. 2	5.7969	5.5445	5.2965	4.6474
	p_z =2	Present (FEM)	6.7681	6.3145	5.9062	4.9503
		Present (ANN)	6.75050294	6.308817	5.897931	4.936934
		Ref. 2	6.7689	6.3154	5.9072	4.9507
	p_z =5	Present (FEM)	7.9433	7.3352	6.7848	5.4531
		Present (ANN)	7.93138505	7.324931	6.776658	5.433469
		Ref. 2	7.9442	7.3363	6.7858	5.4535
L/*h*=20	p_z =0	Present (FEM)	15.0010	15.0010	15.0010	15.0010
		Present (ANN)	14.96800	14.9875	14.9875	14.96200
		Ref. 2	15.0027	15.0036	15.0045	15.0033
	p_z =1	Present (FEM)	23.1850	22.1746	21.1820	18.5877
		Present (ANN)	23.15022	22.14356	21.09092	18.52264
		Ref. 2	23.1877	22.1780	21.1858	18.5895
	p_z =2	Present (FEM)	27.0723	25.2580	23.6248	19.8010
		Present (ANN)	27.02357	25.22769	23.57283	19.76536
		Ref. 2	27.0754	25.2618	23.6288	19.8028
	p_z =5	Present (FEM)	31.7733	29.3410	27.1391	21.8125
		Present (ANN)	31.74788	29.25004	27.09839	21.77324
		Ref. 2	31.7769	29.3452	27.1433	21.8141
			$\bar{\tau}_{xz}(0,0)$			
L/*h*=5	p_z =0	Present (FEM)	0.6000	0.6000	0.6000	0.6000
		Present (ANN)	0.59832	0.59952	0.59892	0.59832
		Ref. 2	0.5827	0.6383	0.6842	0.7502
	p_z =1	Present (FEM)	0.6000	0.6000	0.6000	0.6000
		Present (ANN)	0.59916	0.59916	0.59916	0.59694
		Ref. 2	0.5827	0.6276	0.6614	0.7031
	p_z =2	Present (FEM)	0.5106	0.5106	0.5106	0.5106
		Present (ANN)	0.508609	0.508455	0.509375	0.509732
		Ref. 2	0.4958	0.5280	0.5508	0.5768
	p_z =5	Present (FEM)	0.3930	0.3930	0.3930	0.3930
		Present (ANN)	0.392253	0.391939	0.391349	0.392332
		Ref. 2	0.3816	0.3984	0.4092	0.4205
L/*h*=20	p_z =0	Present (FEM)	0.6000	0.6000	0.6000	0.6000
		Present (ANN)	0.59832	0.5991	0.5991	0.59892
		Ref. 2	0.5827	0.6383	0.6842	0.7502
	p_z =1	Present (FEM)	0.6000	0.6000	0.6000	0.6000
		Present (ANN)	0.5991	0.59814	0.59892	0.59832
		Ref. 2	0.5827	0.6276	0.6614	0.7031
	p_z =2	Present (FEM)	0.5106	0.5106	0.5106	0.5106

Table 5 Continued

L/h=20	p_z =2	Present (ANN)	0.509017	0.509681	0.510192	0.507996
		Ref. 2	0.4958	0.5280	0.5508	0.5768
	p_z =5	Present (FEM)	0.3930	0.3930	0.3930	0.3930
		Present (ANN)	0.392293	0.39245	0.392135	0.392332
		Ref. 2	0.3816	0.3984	0.4092	0.4205

*Ref. 2: Turan (2022)

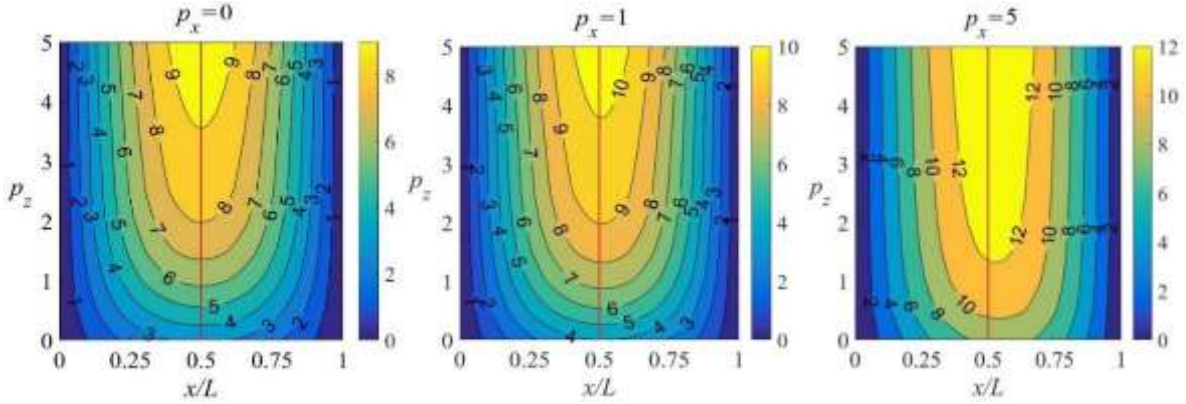

Fig. 4 Non-dimensional displacements of the SS BD-FGBs according to *x/L* and power-law indexes (*L/h*=5)

indicating that slender beams are more prone to experiencing higher normal stresses. On the other hand, shear stresses exhibit an inverse relationship with p_z, decreasing as p_z increases. Interestingly, variations in p_x do not significantly impact shear stress results, which is attributed to the finite element model's reliance on first-order shear deformation theory (FSDT). The comparison with ANN further supports these findings, confirming that the finite element approach, combined with ANN predictions, offers an accurate and robust method for analyzing the stress behavior of BD-FGBs under different power-law conditions. This consistency across different analytical methods enhances the reliability of the proposed model in predicting both normal and shear stresses.

3.2 Parametric study

In this section, a comprehensive analysis of the non-dimensional displacements, as well as normal and shear stresses of bi-directional functionally graded beams (BD-FGBs), is presented for a slenderness ratio of *L/h* = 5. The results are provided for various boundary conditions (BCs), offering a detailed investigation into how different BC configurations influence the mechanical behavior of the beams under static loading conditions. This analysis aims to offer deeper insights into the displacement and stress distributions across the beams, contributing to a more nuanced understanding of their structural performance.

Fig. 4 shows non-dimensional displacements of the SS BD-FGBs according to *x/L* and power-law indexes. According to the figure, displacements increase with increasing power-law indexes. The beam's metallic character increases with the power-law index's increase. The location of the non-dimensional maximum displacements of the SS BD-FGBs is at or very close to the midsection. The location of the $\bar{w}_{max}$ is at the midsection for p_x= 0. For example, for p_z =0 in all cases, *x/L* =0.5 at p_x =0, *x/L* =0.5167 at p_x =1, and *x/L* =0.5533 at p_x =5. For example, for p_x =5 in all cases, *x/L* =0.5533 at p_z =0, *x/L* =0.53 at p_z =1, and *x/L* =0.52 at p_z =5.

Fig. 5 presents variations of the non-dimensional normal stress of the SS BD-FGBs according to *z/h*, *x/L*, and power-law indexes. p_x changes the material property in the *x*-direction, and p_z changes the material property in the *z*-direction. To bring the material property of the beam closer to metal, p_x and p_z must be enlarged. In any beam cross-section in the *x*-direction, the tensile region is at the top, and the compression region is at the bottom. For p_z=0, the material properties in any beam cross-section's tensile and compression regions are the same. In this case, when p_x is increased, the left side of the beam is ceramic, and the ceramic ratio decreases towards the right side. The change in normal stress is minimal to be seen when we consider the boundary condition, and the material properties of the cross-section do not change greatly. However, the effect of p_x is more significant when p_z is nonzero. In this case, with the increase of p_x, the tensile stress decreases, and the compressive stress increases. The tensile stress increases with the increase of p_z. As p_x and p_z are raised, the boundary of the tensile and compressive region changes. Since p_z changes the material properties faster, the variation of p_z is more effective on normal stress than the p_x.

Non-dimensional shear stress of the SS BD-FGBs according to *z/h*, *x/L*, and power-law indexes are given in Fig. 6. For p_z=0; the shear stress distribution is linear. The shear stress is 0.6 at the left edge of the beam, zero at the middle of the beam, and -0.6 at the right edge. When p_z is

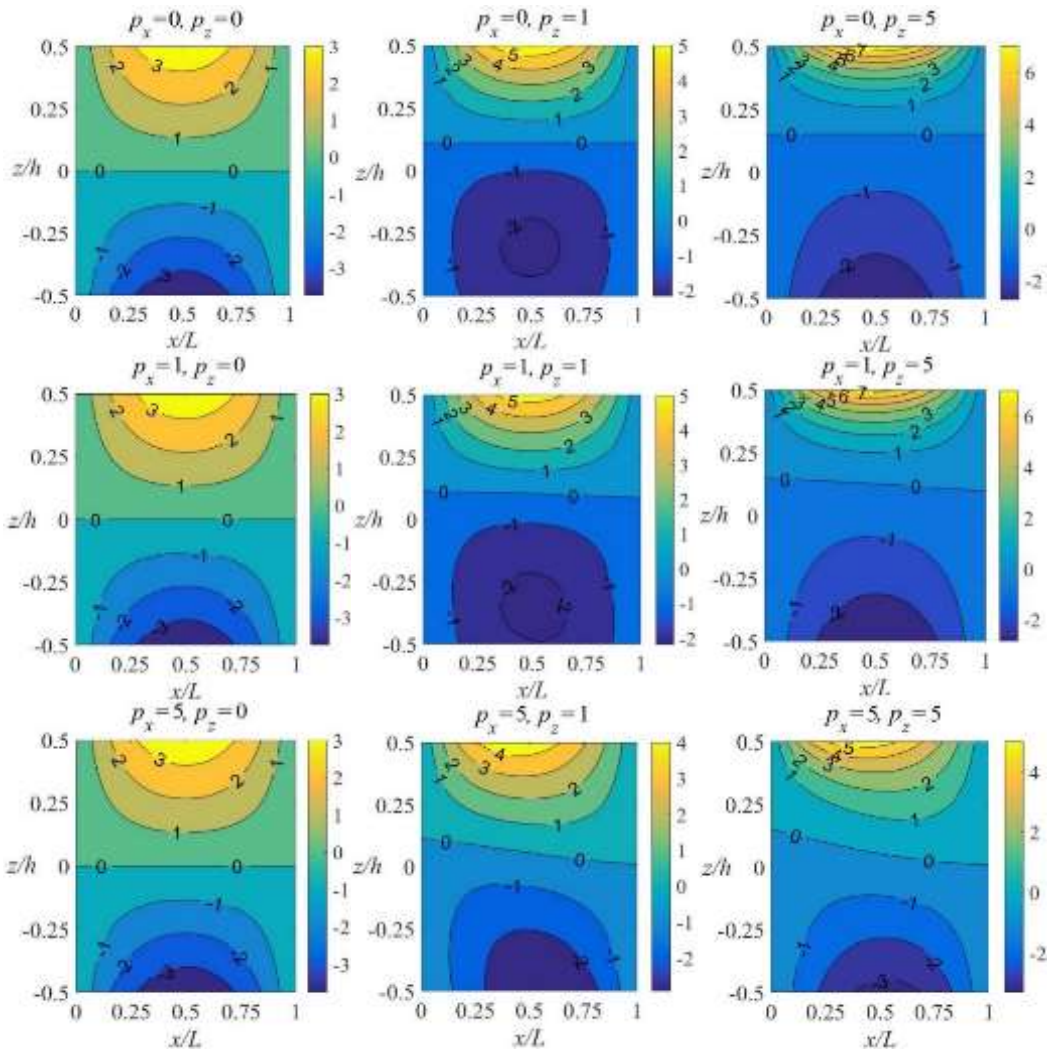

Fig. 5 Non-dimensional normal stress $\bar{\sigma}_{xx}$ of the SS BD-FGBs according to *z/h*, *x/L*, and power-law indexes (*L/h*=5)

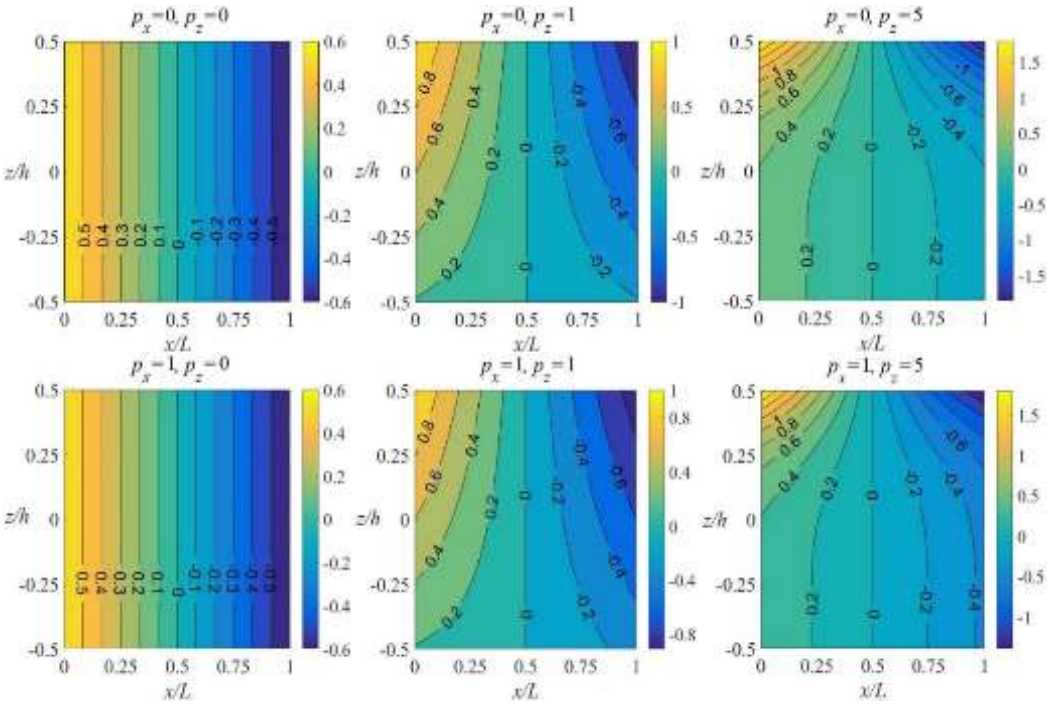

Fig. 6 Non-dimensional shear stress $\bar{\tau}_{xz}$ of the SS BD-FGBs according to *z/h*, *x/L*, and power-law indexes (*L/h*=5)

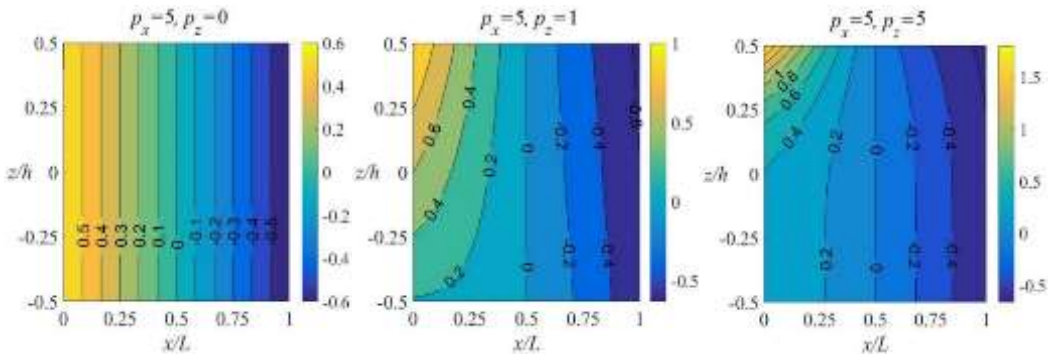

Fig. 6 Continued

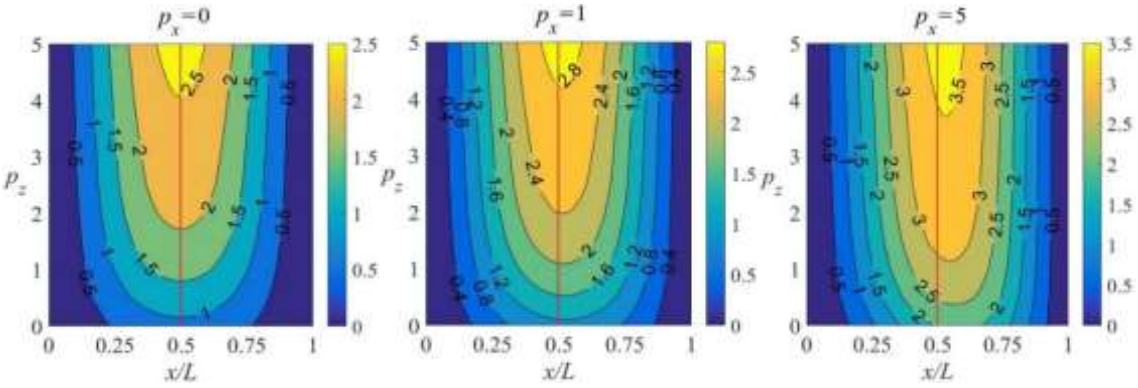

Fig. 7 Non-dimensional displacements of the CC BD-FGBs according to x/L and power-law indexes (L/h=5)

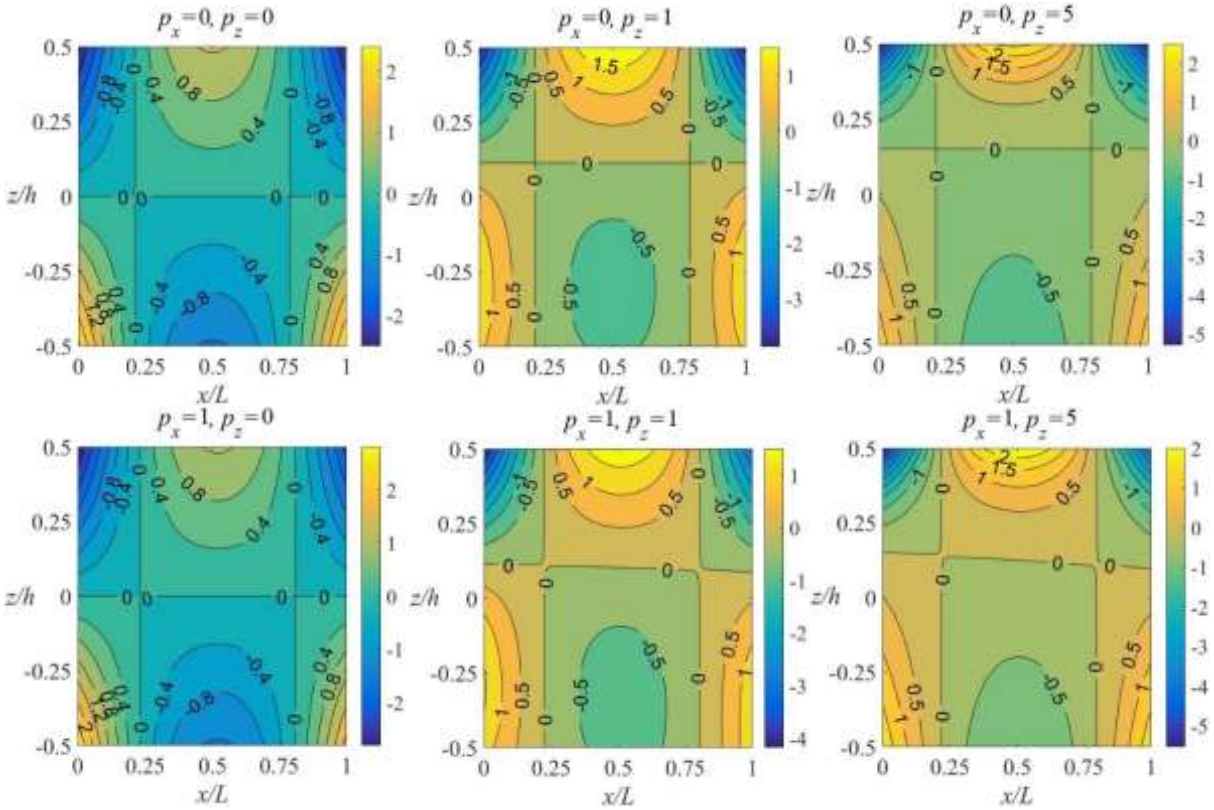

Fig. 8 Non-dimensional normal stress $\bar{\sigma}_{xx}$ of the CC BD-FGBs according to *z/h*, *x/L*, and power-law indexes (*L/h*=5)

nonzero, for example, for p_z=1, with increasing p_x, the shear stress at the left edge of the beam does not change while the shear stress at the right edge decreases. The reason for this is that while the material property of the left edge does not change with the increase in p_x, the material property of the right edge approaches to metal. Also, shear stress

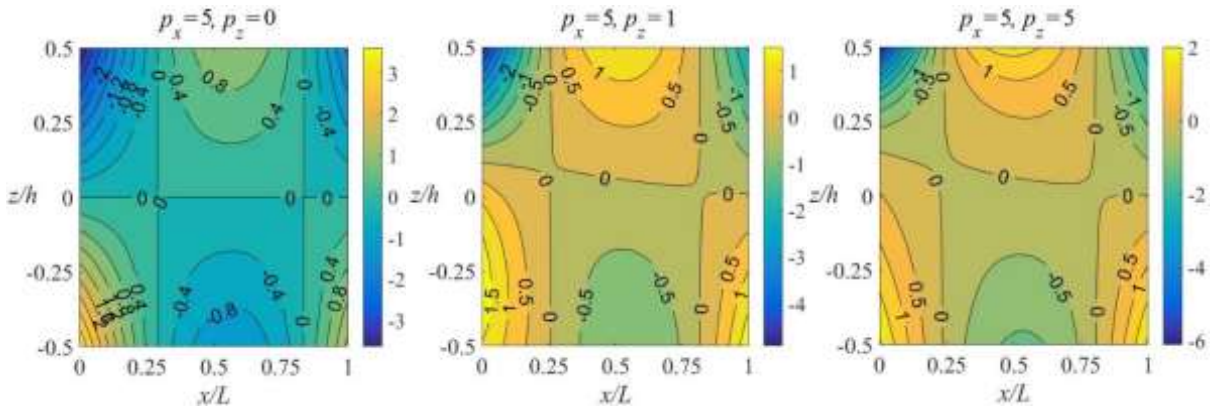

Fig. 8 Continued

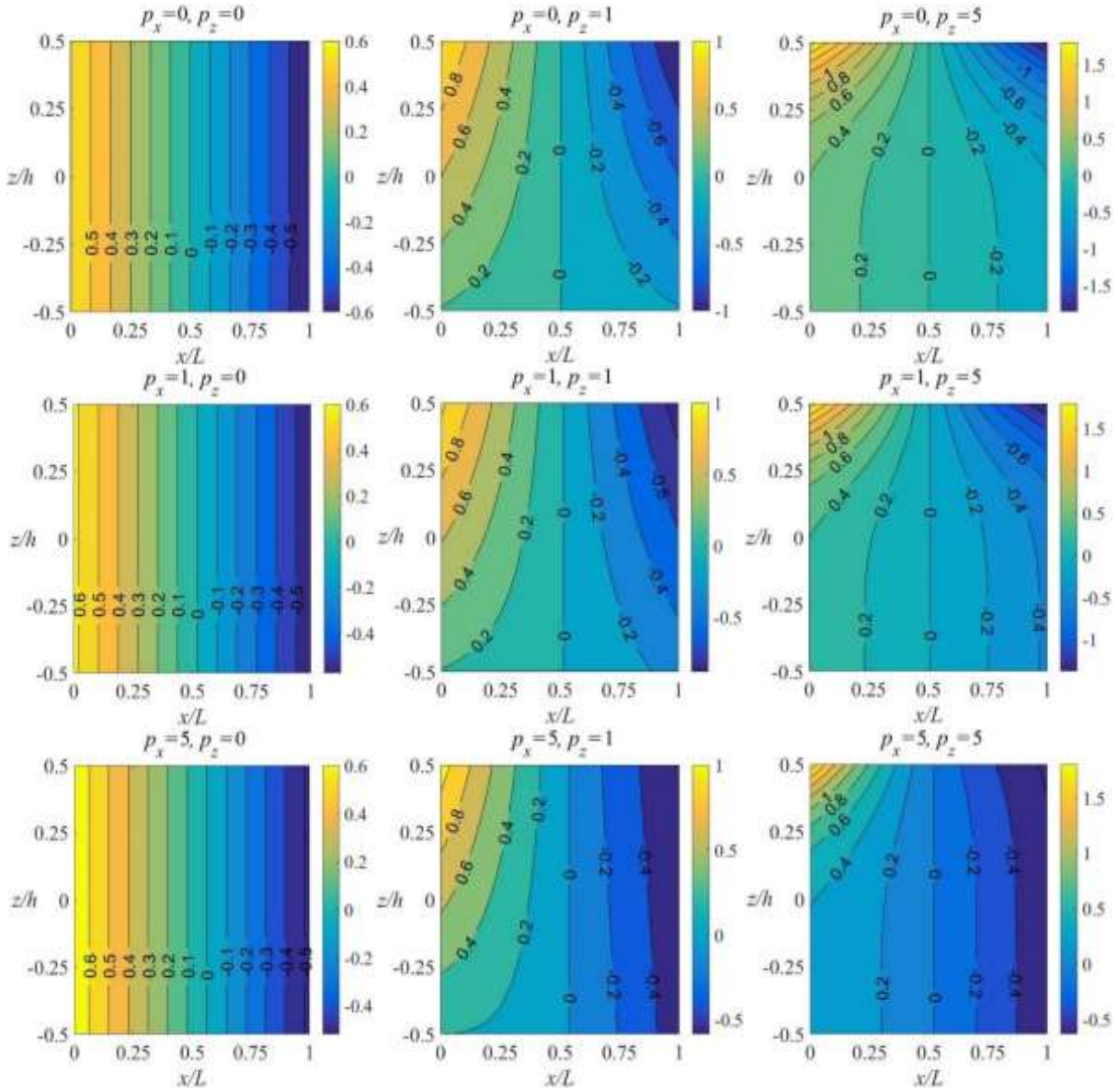

Fig. 9 Non-dimensional shear stress $\bar{\tau}_{xz}$ of the CC BD-FGBs according to *z/h*, *x/L*, and power-law indexes (*L/h*=5)

distribution changes when p_x and p_z are increased. The shear stress increases with not changing p_x and increasing p_z. It is seen that the variation of p_z is more effective than p_x on shear stress.

Non-dimensional displacements of the CC BD-FGBs according to *x/L* and power-law indexes are shown in Fig. 7. The non-dimensional displacements increase with increasing p_x and p_z. At the same time, the maximum

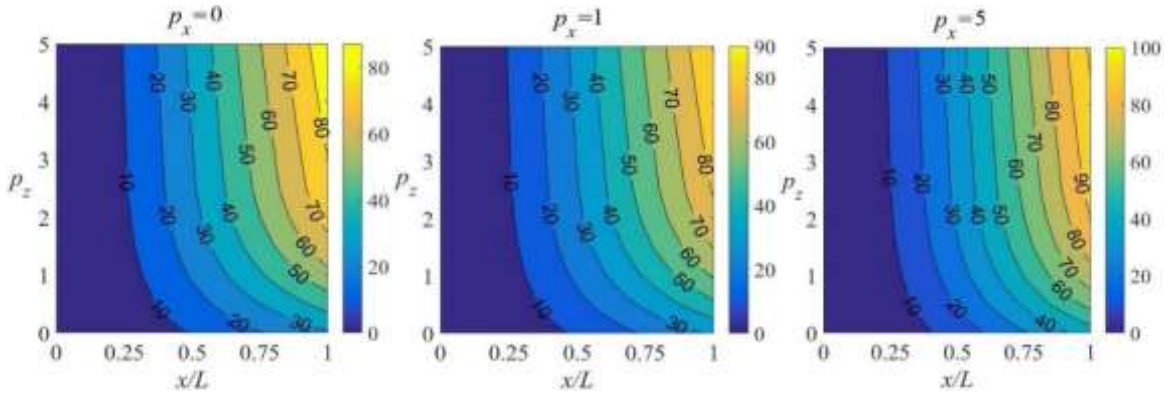

Fig. 10 Non-dimensional displacements of the CF BD-FGBs according to *x/L* and power-law indexes (*L/h*=5)

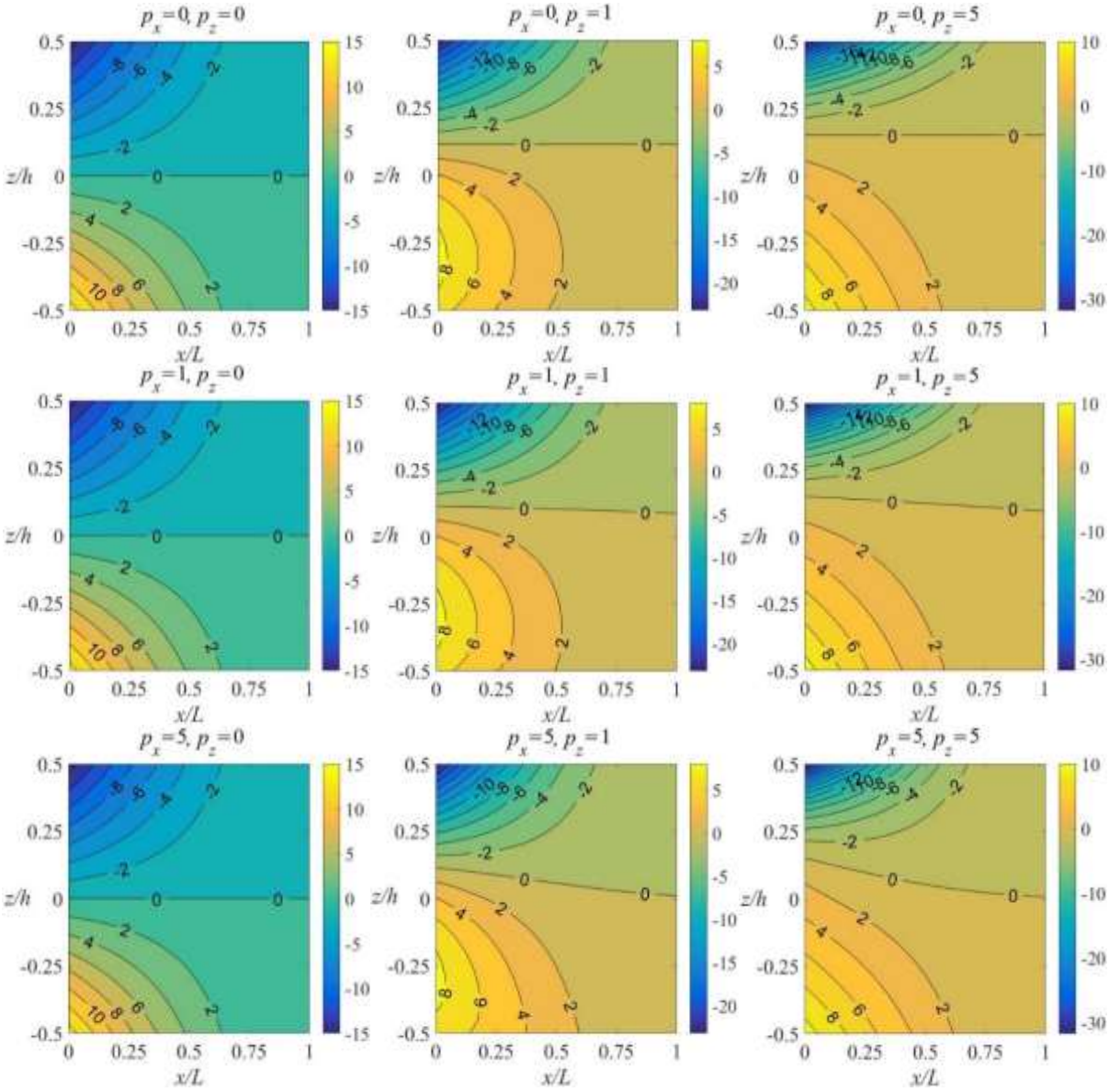

Fig. 11 Non-dimensional normal stress $\bar{\sigma}_{xx}$ of the CF BD-FGBs according to *z/h*, *x/L*, and power-law indexes (*L/h*=5)

displacement is in the midsection of the beam for p_x=0; when the increase of p_x, it moves away right from the midsection. For example, for p_z =0 and p_x =1, the maximum displacement occurs at *x/L*=0.5267. For p_z=0 and p_x=5, the maximum displacement occurs at *x/L*=0.58. Also, for p_x=5, when p_z increases, the maximum displacement approaches the midsection. For example, for p_x=5, *x/L*=0.58 at p_z=0, and *x/L*=0.5267 at p_z=5.

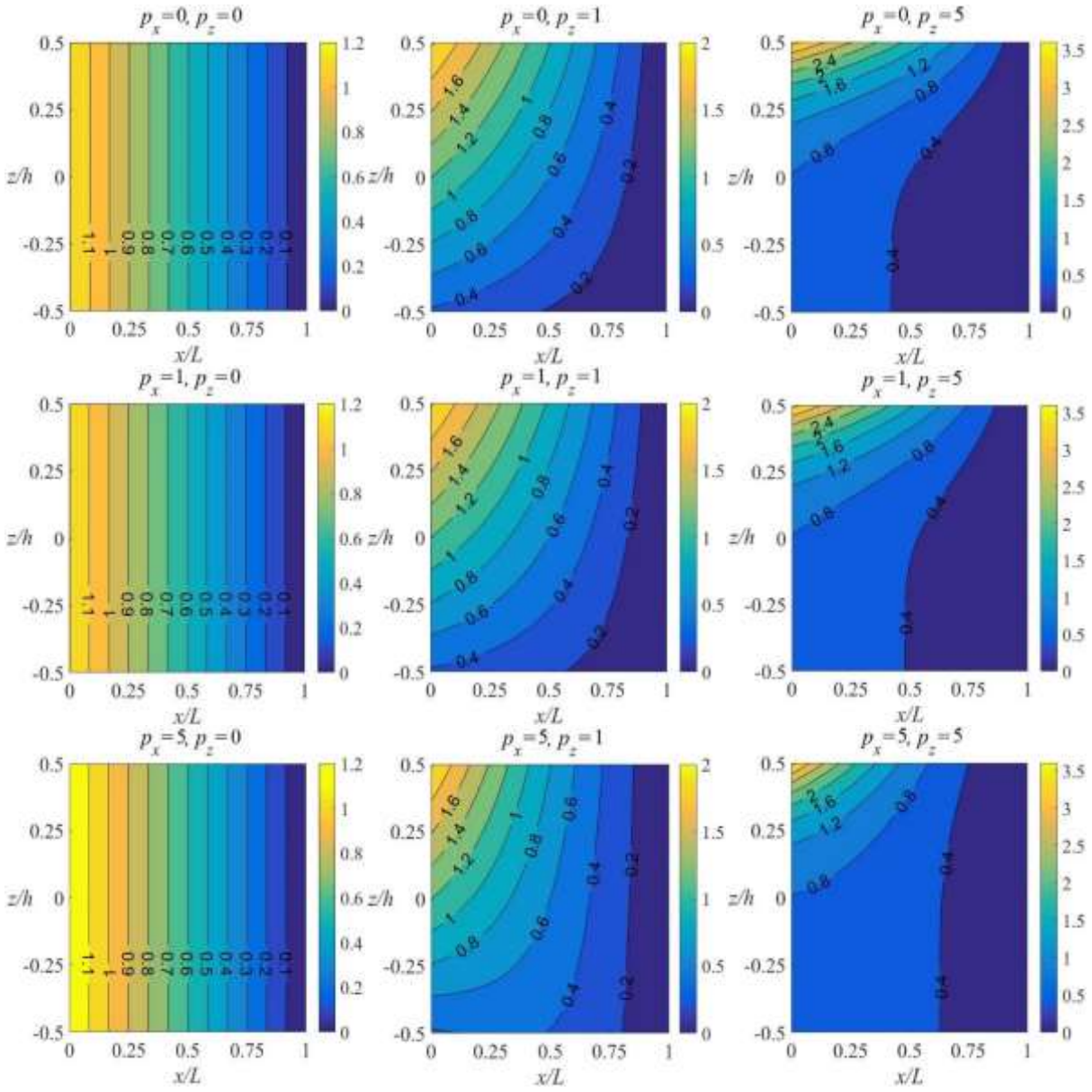

Fig. 12 Non-dimensional shear stress $\bar{\tau}_{xz}$ of the CF BD-FGBs according to *z/h*, *x/L*, and power-law indexes (*L/h*=5)

Fig. 9 presents variations of the non-dimensional shear stress of the CC BD-FGBs according to *z/h*, *x/L*, and power-law indexes. $\bar{\tau}_{xx}$is zero in the midsection for p_x=0 and p_z=0, and this point moves to the right of the midsection with increasing p_x. In the increase in p_x, $\bar{\tau}_{xx}$ increases at the left edge and decreases at the right edge. In this case, the material property is ceramic on the left margin. The ceramic ratio decreases towards the right end of the beam. The maximum $\bar{\tau}_{xx}$increases with increasing p_z on the left and right edges when p_x remains constant. While p_z is constant, increasing px increases the maximum $\bar{\tau}_{xx}$on the left edge and decreases on the right edge.

Fig. 10 shows the non-dimensional displacements of the CF BD-FGBs according to *x/L* and power-law indexes. Non-dimensional displacements increase with increasing p_x and p_z. The maximum displacement always occurs at the free edge, regardless of material properties. It has been observed that the change of p_x and p_z does not affect the location of the maximum displacement in CF BD-FGBs. Still, it is quite effective on the magnitude of the maximum displacement.

The non-dimensional normal stress of the CF BD-FGBs according to *z/h*, *x/L*, and power-law indexes are given in Fig. 11. When p_z=0, even if p_x is increased, the material property on the left edge does not change, so the normal stress value does not change significantly. When p_z=0, 1, or 5, the change of p_x does not affect the location of the maximum normal stress. This is because the maximum and minimum normal stress always occurs on the left edge. The variation of p_x changes the normal stress distribution in the *x*-direction of the beam. In the increase of p_z, the maximum and minimum normal stresses increase.

Fig. 12 presents the non-dimensional shear stress of the CF BD-FGBs according to *z/h*, *x/L*, and power-law indexes.

It was observed that the increase in p_x did not significantly change the shear stress. In the rise of p_z, the maximum shear stress increases significantly. From here, it is seen that p_z is more effective on shear stress than p_x.

4. Conclusions

This paper provides an in-depth analysis of a shear deformable finite element model specifically developed for the static analysis of bi-directional functionally graded beams (BD-FGBs) under various boundary conditions (BCs), employing first-order shear deformation theory (FSDT). The proposed finite element incorporates ten degrees of freedom-three axial, four transverse, and three rotational--distributed across five nodes, allowing for a detailed representation of the beam's behavior. To enhance the reliability and depth of the analysis, the solutions obtained in this study have been rigorously validated and supplemented with Artificial Neural Network (ANN) techniques, offering an innovative approach to structural analysis. The results reveal that variations in the bi-directional properties of functionally graded materials significantly affect the static behavior of the beams. This study uncovers several crucial findings that advance our understanding of BD-FGBs in engineering applications, underscoring the critical relationship between material gradation and structural performance. The proposed finite element accurately predicts the displacements and stresses of functionally graded beams across various BCs and bi-directional material properties, making it a valuable tool for solving such complex problems. It has been established that ANN is an effective method for solving complex problems, such as those involving bi-directional functionally graded beams (BD-FGBs). An increase in power-law indexes in both directions leads to a corresponding increase in deflections. When $p_x = 0$, variations in p_z do not alter the location of the maximum displacement in simply supported (SS) and clamped-clamped (CC) beams. However, at non-zero values of p_x, changes in p_z affect the location of w_{max}. In all scenarios, variations in p_x influence the location of w_{max} in SS and CC beams, which occurs in sections with lower ceramic ratios. In clamped-free (CF) beams, changes in the power-law index have a significant impact on w_{max}, although the location of w_{max} remains constant, consistently occurring at the beam's end. The power-law indexes play a crucial role in shaping the distributions of normal and shear stresses. Notably, the variation of p_z has a more pronounced effect on these stress distributions compared to p_x, as p_z alters the beam's material properties more rapidly.

References

Abd Aziz, A.U., Ammarullah, M.I., Ng, B.W., Gan, H.S., Abdul Kadir, M.R. and Ramlee, M.H. (2024), "Unilateral external fixator and its biomechanical effects in treating different types of femoral fracture: A finite element study with experimental validated model", *Heliyon*, **10**(4), e26660. https://doi.org/10.1016/j.heliyon.2024.e26660

Adiyaman, G and Turan, M. (2024), "Bending and buckling analysis of porous 2D functionally graded beams with exponential material property variation", *Iran J. Sci. Technol. Trans. Civil Eng.*, 0123456789. https://doi.org/10.1007/s40996-024-01508-4

Al-Furjan, M.S.H., Shan, L., Shen, X., Kolahchi, R. and Rajak, D. K. (2022a), "Combination of FEM-DQM for nonlinear mechanics of porous GPL-reinforced sandwich nanoplates based on various theories", *Thin Walled Struct.*, **178**, 109495. https://doi.org/10.1016/j.tws.2022.109495

Al-Furjan, M.S.H., Yin, C., Shen, X., Kolahchi, R., Zarei, M.S. and Hajmohammad, M.H. (2022b), "Energy absorption and vibration of smart auxetic FG porous curved conical panels resting on the frictional viscoelastic torsional substrate", *Mech. Syst. Signal Proc.*, **178**, 109269. https://doi.org/10.1016/j.ymssp.2022.109269

Ammarullah, M.I., Afif, I.Y., Maula, M.I., Winarni, T.I., Tauviqirrahman, M. and Jamari, J. (2022b), "Tresca stress evaluation of Metal-on-UHMWPE total hip arthroplasty during peak loading from normal walking activity", *Mater Today Proc.*, **63**, 143-146. https://doi.org/10.1016/j.matpr.2022.02.055

Ammarullah, M.I., Hartono, R., Supriyono, T., Santoso, G., Sugiharto, S. and Permana, M.S. (2023), "Polycrystalline diamond as a potential material for the hard-on-hard bearing of total hip prosthesis: Von Mises stress analysis", *Biomedicines*, **11**(3), 951. https://doi.org/10.3390/biomedicines11030951

Ammarullah, M.I., Santoso, G., Sugiharto, S., Supriyono, T., Kurdi, O., Tauviqirrahman, M., Winarni, T.I. and Jamari, J. (2022), "Tresca stress study of CoCrMo-on-CoCrMo bearings based on body mass index using 2D computational model", *J. Tribol.*, **33**, 31-38.

Ammarullah, M.I., Santoso, G., Sugiharto, S., Supriyono, T., Wibowo, D.B., Kurdi, O., Tauviqirrahman, M. and Jamari, J. (2022a), "Minimizing risk of failure from ceramic-on-ceramic total hip prosthesis by selecting ceramic materials based on Tresca stress", *Sustainability*, **14**(20), 13413. https://doi.org/10.3390/su142013413

Anh, L.T.N., Ninh, V.T.A., Lang, T.V. and Kien, N.D. (2020), "Free vibration of bidirectional functionally graded sandwich beams using a first-order shear deformation finite element formulation", *J. Sci. Technol. Civil Eng.*, **14**, 136-150. https://doi.org/10.31814/stce.nuce2020-14(3)-12

Aydogdu, M. and Taskin, V. (2007), "Free vibration analysis of functionally graded beams with simply supported edges", *Mater. Des.*, **28**, 1651-1656. https://doi.org/10.1016/j.matdes.2006.02.007

Baseri, V., Jafari, G.S. and Kolahchi, R. (2016), "Analytical solution for buckling of embedded laminated plates based on higher order shear deformation plate theory", *Steel Compos. Struct.*, **21**(4), 883-919. https://doi.org/10.12989/scs.2016.21.4.883

Bazmara, M., Silani, M., Mianroodi, M. and Sheibanian, M. (2023), "Physics-informed neural networks for nonlinear bending of 3D functionally graded beam", *Structures*, **49**, 152-162. https://doi.org/10.1016/j.istruc.2023.01.115

Bennai, R., Atmane, R.A., Bernard, F., Nebab, M., Mahmoudi, N., Atmane, H.A., Aldosari, S.M. and Tounsi, A. (2022), "Study on stability and free vibration behavior of porous FGM beams", *Steel Compos. Struct.*, **45**, 67-82. https://doi.org/10.12989/scs.2022.45.1.067

Chen, D., Zheng, S., Wang, Y., Yang, L. and Li, Z. (2020), "Nonlinear free vibration analysis of a rotating two-dimensional functionally graded porous micro-beam using isogeometric analysis", *Eur. J. Mech. A Solids*, **84**, 104083. https://doi.org/10.1016/j.euromechsol.2020.104083

Chinh, N.V., Inh, L.C. and Ngoc Anh, L.T. (2019), "Elastostatic bending of a 2D-FGSW beam under nonuniform distributed

loads", *Vietnam J. Sci. Technol.*, **57**, 381. https://doi.org/10.15625/2525-2518/57/3/13521
Civalek, Ö., Uzun, B. and Yayli, M.Ö. (2020), "Frequency, bending and buckling loads of nanobeams with different cross sections", *Adv. Nano Res.*, **9**(2), 91-104. https://doi.org/10.12989/anr.2020.9.2.091
Fallah, A. and Aghdam, M.M. (2024), "Physics-informed neural network for bending and free vibration analysis of three-dimensional functionally graded porous beam resting on elastic foundation", *Eng. Comput.*, **40**, 437-454. https://doi.org/10.1007/s00366-023-01799-7
Filippi, M., Carrera, E. and Zenkour, A.M. (2015), "Static analyses of FGM beams by various theories and finite elements", *Compos. Part B Eng.*, **72**, 1-9. https://doi.org/10.1016/j.compositesb.2014.12.004
Furjan, M., Cai, J.X., Shan, L., Shen, X., Yaylacı, M., Rabani bidgoli, M. and Kolahchi, R. (2024a), "Numerical fatigue damage analysis and mathematical modeling of articular cartilage under cyclic load via hyperelasticity theory", *Appl. Math. Model.*, **136**, 115613. https://doi.org/10.1016/j.apm.2024.07.020
Furjan, M., Kolahchi, R. and Yaylacı, M. (2024b), "RFOR-DQHFEM: Hybrid relaxed first-Order reliability and differential quadrature hierarchical finite element method for multi-physics reliability analysis of conical shells", *Thin Wall. Struct.*, **205**, 112583. https://doi.org/10.1016/j.tws.2024.112583
Furjan, M., Kolahchi, R. and Yaylacı, M. (2025), "Energy harvesting capabilities and bandgaps of locally resonant piezoelectric metamaterial panels with self-extraction synchronized circuit", *Appl. Math. Model.*, **141**, 115934. https://doi.org/10.1016/j.apm.2025.115934
Garg, A., Chalak, H.D. and Chakrabarti, A. (2020), "Comparative study on the bending of sandwich FGM beams made up of different material variation laws using refined layerwise theory", *Mech Mater.*, **151**, 103634. https://doi.org/10.1016/j.mechmat.2020.103634
Gul, U. and Aydogdu, M. (2023), "Finite element analysis for longitudinal vibration of nanorods based on doublet mechanics", *Adv. Nano Res.*, **15**(5), 411-422. https://doi.org/10.12989/anr.2023.15.5.411
Hadi Hajmohammad, M., Farrokhian, A. and Kolahchi, R. (2021), "Dynamic analysis in beam element of wave-piercing Catamarans undergoing slamming load based on mathematical modelling", *Ocean Eng.*, **234**, 109269. https://doi.org/10.1016/j.oceaneng.2021.109269
Hadi, A., Nejad, M.Z., Rastgoo, A. and Hosseini, M. (2018), "Buckling analysis of FGM Euler-Bernoulli nano-beams with 3D-varying properties based on consistent couple-stress theory", *Steel Compos. Struct.*, **26**, 663-672. https://doi.org/10.12989/scs.2018.26.6.663
Huang, Y. and Ouyang, Z.Y. (2020), "Exact solution for bending analysis of two-directional functionally graded Timoshenko beams", *Arch Appl Mech.*, **90**, 1005-1023. https://doi.org/10.1007/s00419-019-01655-5
Kahya, V. and Turan, M. (2017a), "Finite element model for vibration and buckling of functionally graded beams based on the first-order shear deformation theory", *Compos Part B Eng.*, **109**, 108-115. https://doi.org/10.1016/j.compositesb.2016.10.039
Kahya, V. and Turan, M. (2017b), "Bending of laminated composite beams by a multi-layer finite element based on a higher-order theory", *Acta Physica Polonica A*, **132**(3), 473-475. https://doi.org/10.12693/APhysPolA.132.473
Kahya, V. and Turan, M. (2018a), "Vibration and stability analysis of functionally graded sandwich beams by a multi-layer finite element", *Compos Part B Eng.*, **146**, 198-212. https://doi.org/10.1016/j.compositesb.2018.04.011
Kahya, V. and Turan, M. (2018b), "Vibration and buckling of laminated beams by a multi-layer finite element model", *Steel Compos. Struct.*, **28**(4), 415-426. https://doi.org/10.12989/scs.2018.28.4.415
Karamanlı, A. (2017a), "Bending behaviour of two directional functionally graded sandwich beams by using a quasi-3d shear deformation theory", *Compos Struct.*, **174**, 70-86. https://doi.org/10.1016/j.compstruct.2017.04.046
Karamanlı, A. (2017b), "Elastostatic analysis of two-directional functionally graded beams using various beam theories and Symmetric Smoothed Particle Hydrodynamics method", *Compos Struct.*, **160**, 653-669. https://doi.org/10.1016/j.compstruct.2016.10.065
Karamanlı, A. and Vo, T.P. (2018), "Size dependent bending analysis of two directional functionally graded microbeams via a quasi-3D theory and finite element method", *Compos Part B Eng.*, **144**, 171-183. https://doi.org/10.1016/j.compositesb.2018.02.030
Karamanli, A. and Vo, T.P. (2021), "Bending, vibration, buckling analysis of bi-directional FG porous microbeams with a variable material length scale parameter", *Appl. Math. Model.*, **91**, 723-748. https://doi.org/10.1016/j.apm.2020.09.058
Keerthiveettil Ramakrishnan, S., Vijayananth, K., Arivendan, A. and Ammarullah, M.I. (2024), "Evaluating the effects of pineapple fiber, potato waste filler, surface treatment, and fiber length on the mechanical properties of polyethylene composites for biomedical applications", *Results Eng.*, **24**, 102974. https://doi.org/10.1016/j.rineng.2024.102974
Khafaji, S.O.W., Al-Shujairi, M.A. and Aubad, M.J. (2020), "Transient analysis of transversely functionally graded Timoshenko beam (TFGTB) in conjunction with finite element method", *Arch Mech Eng.*, **67**, 299-321. https://doi.org/10.24425/ame.2020.131694
Kolahchi, R., Bidgoli, A.M.M. and Heydari, M.M. (2015), "Size-dependent bending analysis of FGM nano-sinusoidal plates resting on orthotropic elastic medium", *Struct. Eng. Mech.*, **55**(5), 1001-1014. https://doi.org/10.12989/sem.2015.55.5.1001
Kolahchi, R., Safari, M. and Esmailpour, M. (2016), "Dynamic stability analysis of temperature-dependent functionally graded CNT-reinforced visco-plates resting on orthotropic elastomeric medium", *Compos. Struct.*, **150**, 255-265. https://doi.org/10.1016/j.compstruct.2016.05.023
Le, C.I., Le, N.A.T. and Nguyen, D.K. (2021), "Free vibration and buckling of bidirectional functionally graded sandwich beams using an enriched third-order shear deformation beam element", *Compos Struct.*, **261**, 113309. https://doi.org/10.1016/j.compstruct.2020.113309
Li, J., Yan, G., Wang, Z., Bouallegue, B. and Alkhalifah, T. (2024), "Optimization of intelligent prosthetic hands using artificial neural networks and nanoscale technologies for enhanced performance", *Adv. Nano Res.*, **17**(4), 369-383. https://doi.org/10.12989/anr.2024.17.4.369
Li, X.F., Wang, B.L. and Han, J.C. (2010), "A higher-order theory for static and dynamic analyses of functionally graded beams", *Arch Appl Mech.*, **80**, 1197-1212. https://doi.org/10.1007/s00419-010-0435-6
Lincy Christy, D., Nagarajan, P. and Madhavan Pillai, T.M. (2020), "Development of elements for analysis of functionally graded beams using applied element method", *Arab J. Sci. Eng.*, **45**, 4053-4065. https://doi.org/10.1007/s13369-020-04375-z
Liu, Q., Peng, K., Zeng, J., Marzouki, R., Majdi, A., Jan, A., Salameh, A.A. and Assilzadeh, H. (2022), "Effects of mining activities on Nano-soil management using artificial intelligence models of ANN and ELM", *Adv. Nano Res.*, **12**(6), 549-566. https://doi.org/10.12989/anr.2022.12.6.549
Lü, C.F., Chen, W.Q., Xu, R.Q. and Lim, C.W. (2008), "Semi-analytical elasticity solutions for bi-directional functionally

graded beams", *Int. J. Solids Struct*., **45**, 258-275. https://doi.org/10.1016/j.ijsolstr.2007.07.018

Madenci, E., Gülcü, Ş. and Draiche, K. (2024), "Analytical nonlocal elasticity solution and ANN approximate for free vibration response of layered carbon nanotube reinforced composite beams", *Adv. Nano Res*., **16**(3), 251-263. https://doi.org/10.12989/anr.2024.16.3.251

Nejad, M.Z. and Hadi, A. (2016b), "Non-local analysis of free vibration of bi-directional functionally graded Euler-Bernoulli nano-beams", *Int. J. Eng. Sci*., **105**, 1-11. https://doi.org/10.1016/j.ijengsci.2016.04.011

Nejad, M.Z., Hadi, A. and Rastgoo, A. (2016a), "Buckling analysis of arbitrary two-directional functionally graded Euler-Bernoulli nano-beams based on nonlocal elasticity theory", *Int J Eng Sci*., **103**, 1-10. https://doi.org/10.1016/j.ijengsci.2016.03.001

Nguyen, D.K., Vu, A.N.T., Le, N.A.T., Pham, V.N. and Alfano, M. (2020), "Dynamic behavior of a bidirectional functionally graded sandwich beam under nonuniform motion of a moving load", *Shock Vib*., **2020**, 8854076. https://doi.org/10.1155/2020/8854076

Nguyen, T.K., Truong-Phong Nguyen, T., Vo, T.P. and Thai, H.T. (2015), "Vibration and buckling analysis of functionally graded sandwich beams by a new higher-order shear deformation theory", *Compos. Part B Eng*., **76**, 273-285. https://doi.org/10.1016/j.compositesb.2015.02.032

Nguyen, T.K., Vo, T.P., Nguyen, B.D. and Lee, J. (2016), "An analytical solution for buckling and vibration analysis of functionally graded sandwich beams using a quasi-3D shear deformation theory", *Compos Struct*., **156**, 238-252. https://doi.org/10.1016/j.compstruct.2015.11.074

Öner, E., Uzun Yaylacı, E. and Yaylacı, M. (2024), "Multi-method examination of contact mechanics in orthotropic layers under gravity", *Mech. Mater*., **1**(1), 1-34. https://doi.org/10.1016/j.mechmat.2024.105036

Özdemir, Ö., Ural, H. and Wahrhaftig, A.D.M. (2024), "Static stability and vibration response of rotating carbon-nanotube-reinforced composite beams in thermal environment", *Adv. Nano Res*., **16**(5), 445-458. https://doi.org/10.12989/anr.2024.16.5.445

Pham, V.N., Nguyen, D.K. and Gan, B.S. (2019), "Vibration analysis of two-directional functionally graded sandwich beams using a shear deformable finite element formulation", *Adv Technol Innov*., **4**, 152-64. https://ojs.imeti.org/index.php/AITI/article/view/4099

Reddy, J.N. and Nampally, P. (2020), "A dual mesh finite domain method for the analysis of functionally graded beams", *Compos. Struct*., **251**, 112648. https://doi.org/10.1016/j.compstruct.2020.112648

Ren, W., Wu, X. and Cai, R. (2022), "A hybrid artificial intelligence and IOT for investigation dynamic modeling of nano-system", *Adv. Nano Res*., **13**(2), 165-174. https://doi.org/10.12989/anr.2022.13.2.165

Kamarian, S., Khalvandi, A., Tran, T.M.N., Barbaz-Isfahani, R., Saber-Samandari, S. and Song, J.I. (2023), "Predicting ESP and HNT effects on the mechanical properties of eco-friendly composites subjected to micro-indentation test", *Adv. Nano Res*., **15**(4), 315-328. https://doi.org/10.12989/anr.2023.15.4.315

Sankar, B.V. (2001), "An elasticity solution for functionally graded beams", *Compos. Sci. Technol*., **61**, 689-696. https://doi.org/10.1016/S0266-3538(01)00007-0

Santoso, G., Ammarullah, M.I., Sugiharto, S., Rachayu, R.M., Mughni, A., Bayuseno, A.P. and Jamari, J. (2024), "Von Mises stress analysis of surgery chair designed for laparoscopic surgeon with lifting mechanism", *AIP Adv*., **14**(4), 045104. https://doi.org/10.1063/5.0188663

Sekban, D.M., Uzun Yaylacı, E., Özdemir, M.E., Yaylacı, M. and Tounsi, A. (2024), "Investigation formability behavior of friction stir welded high strength shipbuilding steel using experimental, finite element and artificial neural network methods", *J. Mater. Eng. Perform*., 1-9. https://doi.org/10.1007/s11665-024-09501-8

Selvamani, R., Thangamuni, P., Yaylacı, M., Özdemir, M.E. and Uzun Yaylacı, E. (2024a), "Nonlinear vibration and parametric excitation of magneto-thermo elastic embedded nanobeam using Homotopy Perturbation Technique", *ZAMM-Z. Angew. Math. Mech*., **104**(12), e202400525. https://doi.org/10.1002/zamm.202400525

Selvamani, R., Ebrahimi, F., Yaylacı, M., Öztürk, Ş. and Uzun Yaylacı, E. (2024b), "Nonlinear poro-thermo-forced vibration in curved sandwich magneto-electro-elastic shells under hygrothermal environment", *Acta Mech*., **235**, 5489-5528. https://doi.org/10.1007/s00707-024-03994-z

Sen, B., Bhowmik, A., Prakash, C. and Ammarullah, M. I. (2024), "Prediction of specific cutting energy consumption in eco-benign lubricating environment for biomedical industry applications: Exploring efficacy of GEP, ANN, and RSM models", *AIP Adv*., **14**(8), 085216. https://doi.org/10.1063/5.0217508

Shafiei, N., Mirjavadi, S.S., MohaselAfshari, B., Rabby, S. and Kazemi, M. (2017), "Vibration of two-dimensional imperfect functionally graded (2D-FG) porous nano-/micro-beams", *Comput. Methods Appl. Mech. Eng*., **322**, 615-632. https://doi.org/10.1016/j.cma.2017.05.007

Shan, L., Furjan, M., Kolahchi, R. and Yaylacı, M. (2025), "Optimization flutter response of laminated smart nanocomposite truncated conical shell under supersonic aerodynamic pressure using hybrid IGWO-DQHFEM", *Aerosp. Sci. Technol*., **156**. https://doi.org/10.1016/j.ast.2024.109766

Şimşek, M. (2015), "Bi-directional functionally graded materials (BDFGMs) for free and forced vibration of Timoshenko beams with various boundary conditions", *Compos Struct*., **133**, 968-978. https://doi.org/10.1016/j.compstruct.2015.08.021

Şimşek, M. (2016), "Buckling of Timoshenko beams composed of two-dimensional functionally graded material (2D-FGM) having different boundary conditions", *Compos Struct*., **149**, 304-314. https://doi.org/10.1016/j.compstruct.2016.04.034

Thai, H.T. and Vo, T.P. (2012), "Bending and free vibration of functionally graded beams using various higher-order shear deformation beam theories", *Int. J. Mech. Sci*., **62**, 57-66. https://doi.org/10.1016/j.ijmecsci.2012.05.014

Truong, T.T., Lee, J. and Nguyen-Thoi, T. (2021), "Multi-objective optimization of multi-directional functionally graded beams using an effective deep feedforward neural network-SMPSO algorithm", *Struct. Multidisc. Optim*., **63**, 2889-2918. https://doi.org/10.1007/s00158-021-02852-z

Truong, T.T., Lee, S. and Lee J. (2020), "An artificial neural network-differential evolution approach for optimization of bidirectional functionally graded beams", *Compos. Struct*., **233**, 111517. https://doi.org/10.1016/j.compstruct.2019.111517

Turan, M. (2022), "Bending analysis of two-directional functionally graded beams using trigonometric series functions", *Arch. Appl. Mech*., **92**, 1841-1858. https://doi.org/10.1007/s00419-022-02152-y

Turan, M. (2024), "Mixed series solution for vibration and stability of porous bi-directional functionally graded beams", *Arch Appl Mech*., **94**(6), 1785-1806. https://doi.org/10.1007/s00419-024-02611-8

Turan, M. and Adiyaman, G. (2023), "A new higher-order finite element for static analysis of two-directional functionally graded porous beams", *Arab. J. Sci. Eng*., **48**(10), 13303-13321. https://doi.org/10.1007/s13369-023-07742-8

Turan, M. and Adiyaman, G. (2024), "Free vibration and buckling analysis of porous two-directional functionally graded beams using a higher-order finite element model", *J. Vib. Eng.*

Technol., **12**(1), 1133-1152. https://doi.org/10.1007/s42417-023-00898-5

Turan, M. and Kahya, V. (2021), "Free vibration and buckling analysis of functionally graded sandwich beams by Navier's method", *J. Fac. Eng. Arch. Gazi Univ*., **36**, 743-757. https://doi.org/10.17341/gazimmfd.599928

Turan, M., Uzun Yaylacı, E. and Yaylacı, M. (2023), "Free vibration and buckling of functionally graded porous beams using analytical, finite element, and artificial neural network methods", *Arch Appl Mech*., **93**(4), 1351-1372. https://doi.org/10.1007/s00419-022-02332-w

Uzun Yaylacı, E. (2022), "Characterization of *Pseudoalteromonas* sp. from aquaculture environment and optimization of fermentation culture parameters by RSM-Based modeling", *Turk. J. Fish. Quat. Sci*., **22**(11). https://doi.org/10.4194/TRJFAS21726

Uzun Yaylacı, E, Öner, E., Yaylacı, M., Özdemir, M.E., Abushattal, A. and Birinci, A. (2022), "Application of artificial neural networks in the analysis of the continuous contact problem", *Struct. Eng. Mech*., **84**(1), 35. https://doi.org/10.12989/sem.2022.84.1.035

Uzun Yaylacı, E., Yaylacı, M., Özdemir, M.E., Terzi, M. and Öztürk, Ş. (2023), "Analyzing the mechano-bactericidal effect of nano-patterned surfaces by finite element method and verification with artificial neural networks", *Adv. Nano Res*., **15**(2). https://doi.org/10.12989/anr.2023.15.2.165

Viet, N.V., Zaki, W. and Wang, Q. (2020), "Free vibration characteristics of sectioned unidirectional/bidirectional functionally graded material cantilever beams based on finite element analysis", *Appl. Math. Mech*., **41**, 1787-1804. https://doi.org/10.1007/s10483-020-2664-8

Wang, X., Guo, X., Babaei, M., Fili, R. and Farahani, H. (2023), "Natural frequency analysis of joined conical-cylindrical-conical shells made of graphene platelet reinforced composite resting on Winkler elastic foundation", *Adv. Nano Res*., **15**(4), 367-384. https://doi.org/10.12989/anr.2023.15.4.367

Yang, Q., Zheng, B., Zhang, K. and Zhu, J. (2013), "Analytical solution of a bilayer functionally graded cantilever beam with concentrated loads", *Arch. Appl. Mech*., **83**(3), 455-466. https://doi.org/10.1007/s00419-012-0693-6

Yarasca, J., Mantari, J.L. and Arciniega, R.A. (2016), "Hermite-Lagrangian finite element formulation to study functionally graded sandwich beams", *Compos Struct*., **140**, 567-581. https://doi.org/10.1016/j.compstruct.2016.01.015

Yaylacı, M., Yaylı, M., Öztürk, Ş., Ay, S., Özdemir, M.E., Uzun Yaylacı, E. and Birinci, A. (2024a), "Examining the contact problem of a functionally graded layer supported by an elastic half-plane with the analytical and numerical methods", *Math. Meth. Appl. Sci*., **47**, 10400-10420 https://doi.org/10.1002/MMA.10129

Yaylacı, M., Öner, E., Adıyaman, G., Öztürk, Ş., Uzun Yaylacı, E. and Birinci, A., (2024b), "Analyzing of continuous and discontinuous contact problems of a functionally graded layer: Theory of elasticity and finite element method", *Mech. Based Des. Struct. Mech*., **52**(8), 5720-5738. https://doi.org/10.1080/15397734.2023.2262562

Yaylacı, M., Uzun Yaylacı, E., Turan, M., Özdemir, M. E., Öztürk, Ş. and Ay, S. (2024c), "Research of the crack problem of a functionally graded layer", *Steel Compos. Struct*., **50**(1), 77-87. https://doi.org/10.12989/scs.2024.50.1.077

Zheng, Y., Jin, H. and Jiang, C. (2022), "Assessment of nonlinear stability of geometrically imperfect nanoparticle-reinforced beam based on numerical method", *Adv. Nano Res*., **13**(2), 113-120. https://doi.org/10.12989/anr.2022.13.2.113

Appendix

Shape functions $\varphi_i(x)$, $\psi_i(x)$ and $\theta_i(x)$ obtained by Lagrange interpolation formula are given in the following:

$$\begin{aligned}
&\varphi_1 = \theta_1 = (1-\xi)(1-2\xi),\\
&\varphi_2 = \theta_2 = 4\xi(1-\xi),\\
&\varphi_3 = \theta_3 = -\xi(1-2\xi),\\
&\psi_1 = \frac{(1-\xi)(1-3\xi)(2-3\xi)}{2},\\
&\psi_2 = \frac{9\xi(1-\xi)(2-3\xi)}{2},\\
&\psi_3 = \frac{-9\xi(1-\xi)(1-3\xi)}{2},\\
&\psi_4 = \frac{\xi(1-3\xi)(2-3\xi)}{2}
\end{aligned} \tag{A1}$$

where $\xi = x/L_e$ and L_e is the element length.

The elements of the mass and stiffness matrices are, respectively,

$$\begin{aligned}
\boldsymbol{m}^{11} &= \frac{I_0 L_e}{30}\begin{bmatrix} 4 & 2 & -1 \\ & 16 & 2 \\ sym & & 4 \end{bmatrix},\\
\boldsymbol{m}^{13} &= \frac{I_1 L_e}{30}\begin{bmatrix} -4 & -2 & 1 \\ & -16 & -2 \\ sym & & -4 \end{bmatrix},\\
\boldsymbol{m}^{22} &= \frac{I_0 L_e}{1680}\begin{bmatrix} 128 & 99 & -36 & 19 \\ & 648 & -81 & -36 \\ & & 648 & 99 \\ sym & & & 128 \end{bmatrix},\\
\boldsymbol{m}^{33} &= \frac{I_2 L_e}{30}\begin{bmatrix} 4 & 2 & -1 \\ & 16 & 2 \\ sym & & 4 \end{bmatrix}
\end{aligned} \tag{A2}$$

$$\begin{aligned}
\boldsymbol{k}^{11} &= \frac{A_0}{3L_e}\begin{bmatrix} 7 & -8 & 1 \\ & 16 & -8 \\ sym & & 7 \end{bmatrix},\\
\boldsymbol{k}^{13} &= \frac{A_1}{3L_e}\begin{bmatrix} -7 & 8 & -1 \\ & -16 & 8 \\ sym & & -7 \end{bmatrix},\\
\boldsymbol{k}^{22} &= \frac{B_0}{40L_e}\begin{bmatrix} 148 & -189 & 54 & -13 \\ & 432 & -297 & 54 \\ & & 432 & -189 \\ sym & & & 148 \end{bmatrix},\\
\boldsymbol{k}^{23} &= \frac{B_0}{120}\begin{bmatrix} 83 & 44 & -7 \\ -99 & 108 & -9 \\ 9 & -108 & 99 \\ 7 & -44 & -83 \end{bmatrix},\\
\boldsymbol{k}^{33} &= \frac{1}{30L_e}\begin{bmatrix} 70A_2 + 4{L_e}^2 B_0 & -80A_2 + 2{L_e}^2 B_0 & 10A_2 - {L_e}^2 B_0 \\ & 160A_2 + 16{L_e}^2 B_0 & -80A_2 + 2{L_e}^2 B_0 \\ sym & & 70A_2 + 4{L_e}^2 B_0 \end{bmatrix}
\end{aligned} \tag{A3}$$

where $[I_0, I_1, I_2] = \int_A \rho(x,z)[1, z, z^2]dA$, $[A_0, A_1, A_2] = \int_A E(x,z)[1, z, z^2]dA$ and $B_0 = \int_A KG(x,z)dA$